Development of Novel Muffler Configurations for Range Extended Hybrid Electric Vehicles

M.Tech Thesis

by

Sadanand Gautam

Department of Mechanical Engineering

Indian Institute of Technology Indore

June 2024

Development of Novel Muffler Configurations for Range Extended Hybrid Electric Vehicles

A Thesis

Submitted in partial fulfillment of the

requirments for the award of the degree

of

Master of Technology

by

Sadanand Gautam

Department of Mechanical Engineering

Indian Institute of Technology Indore

June 2024

INDIAN INSTITUTE OF TECHNOLOGY INDORE

CANDIDATE'S DECLARATION

I hereby certify that the work which is being presented in the thesis entitled **"Development of Novel Muffler Configurations for Range Extended Hybrid Electric Vehicles"** in the partial fulfillment of the requirements for the award of the degree of **MASTER OF TECHNOLOGY** and submitted in the **DEPARTMENT OF MECHANICAL ENGINEERING, Indian Institute of Technology Indore** is an authentic record of my own work carried out during the time period from May 2023 to May 2024 under the supervision of **Dr. K. M. Kumar**, Assistant Professor, Department of Mechanical Engineering, Indian Institute of Technology Indore.

The matter presented in this thesis has not been submitted by me for the award of any other degree of this or any other institute.

Sadanand Gautam
19-06-2024
Sadanand Gautam
(Student)

This is to certify that the above statement made by the candidate is correct to the best of my knowledge.

K. M. Kumar

Dr. K. M. Kumar
(Thesis Supervisor)

Mr. Sadanand Gautam has successfully given his M.Tech. Oral Examination held on May 30, 2024.

K. M. Kumar

Signature of the Supervisor of M.Tech. thesis — Convener, DPGC

Date: June 19, 2024 — Date:

Dedicated to my family for their love, care, and blessings. . . !

ACKNOWLEDGEMENTS

Above all, I would like to thank God for the life experiences, accomplishments, and failures that have shaped me into the person I am today. My sincere gratitude goes to my parents and siblings for their love, affection, and belief in me. The entire M. Tech. program has been an amazing experience for me, not only in terms of acquiring skills in the field of noise control, but also in terms of learning a lot more about research methods, a positive attitude towards life, and interpersonal relationships. I would like to express my sincere gratitude to my mentor **Dr. K. M. Kumar**. I am truly thankful for his invaluable guidance, which has played a significant role in shaping me into a well-rounded engineer and introducing me to the realm of NVH (Noise, Vibration, and Harshness). Throughout my journey as a graduate student, **Dr. K. M. Kumar** has generously provided me with numerous opportunities and unwavering support, both professionally and personally. Moreover, I have thoroughly enjoyed our diverse conversations on various subjects over last one year, finding them both enjoyable and enlightening. I also want to thank **Mr. Gaurav Sharma** (Ph.D. scholar, TAAL Lab) for helping me throughout my whole M. Tech. Journey at IIT Indore. I also want to thank **Mr. Asif Nisar** (M.S. student, TAAL Lab) for providing me valuable suggestions regarding the presentation and thesis work. I also want to thank **Evaluation Committee Members** for providing me the invaluable suggestions regarding the project and the presentation. My experience as an M. Tech. student at IIT Indore has been profoundly shaped by the camaraderie of my classmates.

Thanks a lot, everyone. . . !
SADANAND GAUTAM

Abstract

The demand for range-extended hybrid electric vehicles is increasing year by year over battery based vehicles. The range-extended hybrid electric vehicles combine battery and internal combustion (IC) engine to provide the benefit of both battery and IC engine. Despite their advantages, hybrid vehicles also present some challenges. One significant issue arises when the battery gets discharged then a switch from battery power to IC engine power becomes a necessity, which causes a sudden change in noise levels within the passenger cabin, and this disturbs the acoustic comfort and experience of passengers. The abrupt noise shift happens when the quiet operation of the electric motor transitions to the louder IC engine, resulting in noticeable cabin noise. To eliminate this issue, mufflers with a high values of transmission loss (TL), especially at low frequencies as well as wideband TL spectra are essential to ensure a smooth and seamless transition between power sources.

Wideband transmission loss (TL) spectrum can be obtained from a simple straight flow muffler by making acoustical lengths of the extended inlet and outlet pipe equal to half and quarter chamber lengths, inside the chamber. The physical lengths of the extended inlet and outlet pipes are less than that of the desired acoustic lengths due to the evanescent higher-order modes generated at the area discontinuities. However, the drawbacks of such mufflers are significant back pressure and the generation of aerodynamic noise around area discontinuities. However, fortunately, creating a perforated bridge between the extended inlet and extended outlet, these two drawbacks can be avoided. The envelope of the TL spectrum which excludes the sharp peaks is of the great importance to design muffler configurations for working with varying speeds of IC engines. Wideband transmission loss spectrum can be obtained by a small elliptical chamber by placing the inlet and outlet ports at certain locations on major axis and minor axis. However, in the plane wave region, double-tuned muffler configuration with perforated bridge between the inlet and outlet pipes an axially long has more TL values in the low-frequency region as compared with the short elliptical chamber. In the present study, double-tuning of the eccentric perforated tube resonator muffler is done. Transmission loss (TL) spectra of short elliptical chamber muffler with different port locations are compared. Fi-

nally, two combination muffler configurations with an axially short chamber placed in between the two axially long double-tuned eccentric/concentric perforated tube resonators. Moreover, the performances of the combination mufflers with equal lengths of two axially long chambers and different lengths of two axially long chambers are also investigated. The variation of the TL spectra was also analyzed with different port locations of the short chamber. Acoustic analysis of the designed combination mufflers are done by two approaches, namely, transfer matrix method (TMM), and 3-D finite element method (FEM). It is observed that the comparison of the TL spectra computed by 1-D TMM and 3-D FEM are excellent till 800 Hz. Therefore, the 1-D TMM can be applied for synthesis of proposed muffler configurations in the present study.

Contents

List of Figures

List of Tables

Acronyms

TL	Transmission Loss
IL	Insertion loss
LD	Level Difference
SPL	Sound Pressure Level
SEC	Simple Expansion Chamber
CTR	Concentric tube resonator
OTR	Offset Tube Resonator
WHO	World Health Organization
TMM	Transfer Matrix Method
DTOTR	Double Tuned Offset Tube Resonator
DTCTR	Double Tuned concentric Tube Resonator

Chapter 1

Introduction

Noise is defined as "any unwanted sound." The World Health Organization (WHO) has described noise pollution as a significant threats that can lead to short-term and long-term health issues. However, these noise pollution is often underestimated. These health problems may include cardiovascular effects, sleep disturbances, decreased workplace performance, and hearing loss.

Vehicles have played a crucial role in the development of human civilization, but they have also been significant contributors to noise pollution. The common problem of IC engines automotive vehicles running on high unmuffled exhaust sound pressure levels. However, over the years, very efficient muffler configurations have been developed which reduce the radiated exhaust sound pressure level. International and national organizations have established standards for automobile manufacturers to design vehicles that adhere to specified noise emission limits.

In automobiles, the noise generated by IC engine exhaust is reduced by utilizing mufflers. Therefore, mufflers play a significant role in mitigating IC engine exhaust noise. Design of mufflers are subjected to constraints on optimization of overall IL, volume of muffler, and backpressure. The following section provides a detailed description of mufflers, including their classification and other relevant details.

1.1 Muffler

Mufflers, also known as silencers, are components of an exhaust system that reduce the noise of IC engines. The noise reduction by the mufflers is achieved by absorption of sound, reflection of the sound back to the source, and cancellation of sound waves coming from two different paths. Besides automobiles, mufflers are used to attenuate sound produced by various industrial machinery such as compressors, turbines, and blowers. Figure 1.1 shows the schematic diagram of a typical muffler used in automobiles.

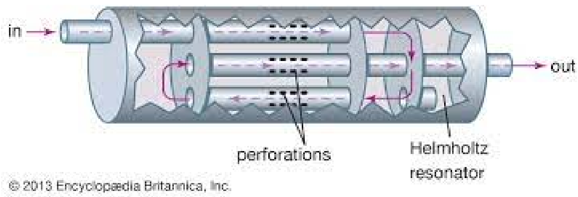

Figure 1.1: Schematic diagram of a typical muffler [1]

Figure 1.2 shows the first patented muffler by Reeves brothers in 1897 [2], which marked a significant advancement in automotive technology. In early 20^{th} century, car engines used to produce considerable noise, prompting the need for effective noise-reduction solutions. Their design used sound-absorbing materials and intricate internal baffles to reduce engine noise significantly. This innovation improved the driving experience by making vehicles quieter and set the stage for future developments in exhaust system technology.

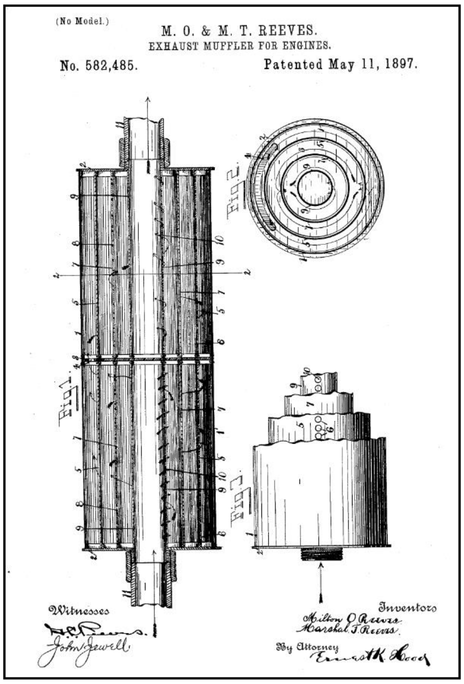

Figure 1.2: First patented muffler by Reeves brothers [2]

1.2 Classification of Muffler

Mufflers, also known as silencers, are classified based on their internal design and function in reducing noise from the exhaust systems of engines. The three different types of mufflers are discussed in the following subsection:

1.2.1 Reactive muffler

The primary function of acoustic elements in a reactive muffler is to reflect acoustic waves back to their source. When an acoustic wave crosses a boundary between two areas with different acoustic impedances, most of the acoustic energy is reflected back to the source. The greater the impedance difference, the more significant the reflection. Additionally, the reflected wave undergoes a phase change, creating destructive interference with the incident wave. These mechanisms enable reactive mufflers to reduce the transmitted acoustic energy from a sound source [3].

1.2.2 Absorptive muffler

Absorptive mufflers, also known as the dissipative mufflers, use specialized materials to absorb sound energy. Sound waves lose their energy as it is converted into heat by absorptive material. Typically, an absorptive muffler consists of a straight perforated pipe with a circular cross-section, housed within a steel casing. Glass wool is a common choice for the absorptive material [3].

Compared to a reactive muffler, an absorptive muffler generates lower back pressure. However, vehicles equipped with absorptive mufflers are not very much effective at low-frequency noise (20 Hz - 500 Hz). While Reactive mufflers utilize resonating chambers to target specific frequencies for control, absorptive mufflers excel at attenuating higher frequencies.

1.2.3 Combination muffler

Combination mufflers, also known as hybrid mufflers, integrate both absorptive and reactive elements to optimize noise reduction across various engine conditions. By combining materials like fiberglass for absorbing sound waves and chambers with baffles or resonators for reflecting and canceling out specific frequencies, these mufflers aim to achieve comprehensive noise attenuation. This design approach addresses the limitations of purely absorptive or reactive mufflers alone, offering a balanced solution that enhances durability, performance, and effectiveness in reducing exhaust noise across a wide range of driving scenarios.

1.3 Muffler Performance Parameters

Exhaust system performance can be assessed using a variety of parameters, each of which provides a different perspective on how effective the system is, despite this, choosing the right performance parameter is essential to arriving at reliable results. The three important parameters are discussed below [4].

1.3.1 Transmission Loss

The difference in the sound power level between the transmitted wave at the outlet with anechoic termination and the incident wave at the muffler inlet is known as transmission loss (TL). Expression of TL for different inlet and outlet pipes cross-section area is given by Eq. 1.1.

$$TL = 20\log_{10}\left(\frac{|p_i|}{|p_t|}\right) + 10\log\left(\frac{S_i}{S_o}\right) = 20\log_{10}\left(\frac{|p_1 + Y_1 v_1|}{|2Y_2 v_2|}\right) + 10\log_{10}\left(\frac{S_i}{S_o}\right) \tag{1.1}$$

Here S_i and S_o represent the cross-sectional areas of the inlet and outlet port respectively. Subscripts '1' and '2' stand for the inlet and outlet pipes. p_1 is the acoustic pressure in the inlet pipe, whereas v_1 and v_2 are acoustic mass velocities in the inlet pipe and the outlet pipe, respectively. The second term in the TL equation becomes zero if the cross-sectional areas of the inlet and output port are same. Y_1 and Y_2 are characteristic impedances of the inlet pipe and the outlet pipe, respectively.

1.3.2 Insertion Loss

Insertion Loss (IL), is the difference between the acoustical power level radiated without any muffler and with muffler. Expression of IL is given by Eq. 1.2, where L_{w1} denotes the radiated sound power level in dB without any muffler and L_{w2} denotes the radiated sound power level in dB with the muffler.

$$IL = L_{w1} - L_{w2} = 10\log_{10}\left(\frac{W_1}{W_2}\right) \tag{1.2}$$

1.3.3 Level Difference

The level difference (or noise reduction) is defined as the difference in sound pressure levels at two arbitrary locations in the muffler's inlet pipe and the outlet pipe. Unlike the TL, there is no need for the anechoic termination for the measurement/computation of level difference.

$$LD = 20\log_{10}\left(\frac{p_i}{p_o}\right) \tag{1.3}$$

1.4 Acoustic wave propagation theory

Acoustic wave propagation theory describes the behavior of sound waves as they travel through a medium. Sound waves propagate through compressions and rarefactions of the medium's molecules, characterized by parameters like wavelength, frequency, amplitude, and velocity. In the following subsections, plane wave propagation and three-dimensional wave propagation in an inviscid stationary medium are discussed.

1.4.1 Plane waves in an inviscid stationary medium

Only plane wave propagates in ducts before the cut-on of any possible higher order mode [4]. For the plane wave propagation, the two-state variables, particle velocity (u) and acoustic pressure (p), are constant at all points of a cross-section. The 1-D wave equation for acoustic pressure(p) is given by Eq. 1.4. The plane wave equation is derived by mass continuity, momentum conservation, and energy equations to a control volume of length dx.

$$\frac{\partial^2 p}{\partial t^2} - c^2\frac{\partial^2 p}{\partial x^2} = \left(\frac{\partial}{\partial t} + c\frac{\partial}{\partial x}\right)\left(\frac{\partial}{\partial t} - c\frac{\partial}{\partial x}\right)p = 0 \tag{1.4}$$

Equation 1.5 gives the acoustic pressure in terms of the spatial coordinates(x) and time(t) for the plane wave condition. The time dependence is assumed $e^(j\omega t)$. Here, C_1 represents the coefficient of the progressive wave, C_2 represents the coefficient of the reflective wave, k_0 is the wave number, and ω is the frequency in radian per second. The relation between k_0, ω, sound speed(c), and wavelength(λ) is given by Eq. 1.6.

The first and second term of Eq. 1.5 are the progressive wave moving in forward direction and backward direction, respectively.

$$p(x,t) = (C_1 e^{-jk_0x} + C_2 e^{jk_0x}) e^{j\omega t} \tag{1.5}$$

$$k_0 = \frac{\omega}{c} = \frac{2\pi}{\lambda} \tag{1.6}$$

The particle velocity (u) also satisfies the wave equation as acoustic pressure using momentum equation and Eq. 1.5, one can find the particle velocity (u) as a function of x and t given by Eq. 1.7. Here, Z_0 is the medium's characteristic impedance, which is ratio of acoustic pressure and particle velocity of a plane progressive wave. Expression of the characteristic impedance of the medium is given by Eq. 1.8, where ρ and c are the density of the medium, and sound speed respectively.

$$u(x,t) = \frac{1}{z_0}(C_1 e^{-jk_0x} - C_2 e^{jk_0x}) e^{j\omega t} \tag{1.7}$$

$$z_o = \frac{p}{u} = \rho c \tag{1.8}$$

Instead of particle velocity (u), mass velocity (v) is more frequently used as the second state variable in muffler analysis. Particle velocity can be converted to mass velocity by multiplying ρs. Expression of mass velocity is given by Eq. 1.9. Here, Y_0 represents the characteristic impedance of the tube. Expression of the tube's characteristic impedance is given by Eq. 1.10. Where S stands for the tube's cross-sectional area.

$$v(x,t) = \frac{1}{Y_0}(C_1 e^{-jk_0x} - C_2 e^{jk_0x}) e^{j\omega t} \tag{1.9}$$

$$Y_o = \frac{p}{V} = \frac{c}{S} \tag{1.10}$$

1.4.2 Three-Dimensional waves in an inviscid stationary medium

After the cut-on of possible first higher-order mode, acoustic pressure field can be described by the 3-D wave equation given by Eq. 1.11 can be derived using similar method as the 1D wave equation, but it takes into account the variations in all three spatial dimensions.

$$\frac{\partial^2 p}{\partial t^2} - c^2 \nabla^2 p = 0 \tag{1.11}$$

where,

$$\nabla^2 = \frac{\partial^2}{\partial x^2} + \frac{\partial^2}{\partial y^2} + \frac{\partial^2}{\partial z^2} \qquad \text{for the cartesian coordinate system,}$$

$$\nabla^2 = \frac{\partial^2}{\partial r^2} + \frac{1}{r}\frac{\partial^2}{\partial r} + \frac{1}{r^2}\frac{\partial^2}{\partial \theta^2} + \frac{\partial^2}{\partial z^2} \qquad \text{for the cylindrical coordinate system,}$$

and

$$\nabla^2 = \frac{2}{h^2[\cosh(2\zeta) - \cos(2\eta)]}\left(\frac{\partial^2}{\partial \zeta^2} + \frac{\partial^2}{\partial \eta^2}\right) + \frac{\partial^2}{\partial z^2} \qquad \text{for the elliptical coordinate system.}$$

Expressions of acoustic pressure for rectangular ducts, cylindrical ducts, and elliptical ducts are given by Eq. 1.12, 1.13, and 1.14, respectively.

$$p(x,y,z,t) = \sum_{m=0}^{\infty}\sum_{n=0}^{\infty} \cos\left(\frac{m\pi x}{b}\right)\cos\left(\frac{n\pi y}{h}\right)(C_{1,m,n}e^{-jk_{z,m,n}z} + C_{2,m,n}e^{jk_{z},m,nz})e^{j\omega t} \tag{1.12}$$

$$p(r,\theta,z,t) = \sum_{m=0}^{\infty}\sum_{n=1}^{\infty} J_m(k_{r,m,n}r))e^{jm\theta}(C_{1,m,n}e^{-jk_{z,m,n}z} + C_{2,m,n}e^{jk_{z,m,n}z})e^{j\omega t} \tag{1.13}$$

$$\begin{aligned} p(\zeta,\eta,z,t) = \Bigg[&\sum_{m=0}^{\infty}\sum_{n=1}^{\infty} Ce_m(\zeta,q_{m,n})ce_m(\eta,q_{m,n}))(C_{m,n}^1 e^{-jk_{z,m,n}^+ z} + C_{m,n}^2 e^{jk_{z,m,n}^- z}) + \\ &\sum_{m=0}^{\infty}\sum_{n=1}^{\infty} Se_m(\zeta,\bar{q}_{m,n})se_m(\eta,\bar{q}_{m,n}))(S_{m,n}^1 e^{-j\bar{k}_{z,m,n}^+ z} + S_{m,n}^2 e^{j\bar{k}_{z,m,n}^- z})\Bigg] e^{j\omega t} \end{aligned} \tag{1.14}$$

1.5 Thesis outline:

The organization of the thesis which consists of six chapters is given below.

- **Chapter 1. Introduction:** A brief introduction on muffler is given in this chapter.
- **Chapter 2. Literature review:** A brief literature review on Double tuning of muffler

configuration, and effect of inlet/outlet port location in the short elliptical chamber is presented in this chapter.

- **Chapter 3. 3-D FEM analysis of muffler configurations:** In this chapter, 3-D FEM is applied to analyze the muffler configurations.

- **Chapter 4. Plane-wave analysis of muffler configuration by 1-D TMM:** In this chapter, 1-D TMM is applied to analyze and synthesize the muffler configurations.

- **Chapter 5. Results and Discussions:** In this chapter, results obtained by 1-D TMM and 3-D FEM are discussed.

- **Chapter 6. Conclusion and Future work:** In this chapter, conclusion of the present study is presented, and the direction for the future work are given.

Chapter 2

Literature review

Noise generated by internal combustion engines are exhaust noise, intake noise and body noise. The body noise is produced by the vibration of engine surfaces and connecting parts. Exhaust and intake noise are produced due to the pulsating gas flow in the exhaust system and intake system, respectively. The exhaust and intake noise can be dealt with use of efficient mufflers. The simple expansion chamber (SEC) and reversing chamber muffler (RCM) are the simplest mufflers for opposite ends inlet-outlet and same end inlet-outlet muffler configurations, respectively. However, the SEC and RCM have periodic domes in transmission loss (TL) curves making them unsuitable for reducing vehicle exhaust noise [4]. The TL troughs of the SEC and RCM can be lifted by extending one of the inlet duct and outlet duct acoustic lengths by L/2, and other by L/4 into the chamber. Selamet and Ji [5] investigated the effects of chamber length and extended duct lengths on acoustic attenuation performance, as well as the effect of inlet and outlet port locations on wave propagation and attenuation by analytically, computationally and numerically. The sudden expansion and contraction takes place at the junction of the inlet and outlet pipes, chamber and annular region surrounding the inlet/outlet pipes. The transmission loss spectrum of an extended inlet-outlet muffler computed by plane wave analysis does not match with either numerically computed TL spectrum or measured TL spectrum for the same extended lengths used in plane wave analysis, 3-D FEM, and measurement. The reason for difference in TL spectra even before the cut-on of first possible higher-order mode is that the evanescent higher-order modes that are generated at junction. The effect of higher-order evanescent waves can be approximated as inline inertance which in turn can be approximated as increase in lengths which are known as end-corrections [5]. The end-correction for the sudden area discontinuities of concentric cylinder were analytically studied by Karal [6], whereas numerical computation of end-correction for concentric discontinuities, and eccentric discontinuities were done by Sahasrabudhe et al. [7]. End-correction for extended-duct and perforated-duct mufflers was computed numerically by torregrosa et al. [8]. The effect of the sudden expansion and sudden contraction was given in the form of parametric expression by torregrosa et al. on end correction as a function of the diameter ratio (D/d). The expression was used for one-dimensional model which obviates the need of 3-D FEA. Also, parametric expression of end-correction for perforated muffler as a function of D/d was given by torregrosa et al. [8]. Transmission loss values of a double-tuned extended inlet and outlet muffler are higher as compared to the simple expansion chamber muffler till the plane wave frequency limit [9]. However, as per the lumped flow resistance network analysis, the head loss are same in both mufflers. The use of the perforated bridge between the extended inlet and extended outlet pipe can remove the problem of the head loss because of the sudden area discontinuities and at the same time, the muffler can be double-tuned as like extended inlet-outlet muffler [9]. A parametric expression for the end correction of extended inlet outlet pipes in terms of wall thickness to diameter ratio (w/d) and the diameter ratio (D/d), was proposed by Chaitanya and Munjal [10]. Parametric expression for the differential length of perforated pipe of a double-tuned concentric tube resonator (DTCTR) was given by Chaitanya and Munjal [11]. The difference in the geometric and the acoustic and the geometrical lengths in the case of CTR due to the inertance of the holes. These differential lengths have been precisely calculated by comparing the resonance peaks predicted through plane wave or 1-D analysis with those obtained by 3-D FEA, and corroborated with measurement Chaitanya and Munjal [11]. A parametric study for differential lengths of double-tuned concentric tube resonator (DTCTR) was carried by Ramya and Munja [12]. They gave the regressed parametric expression for differential lengths and end corrections of DTCTR as function of seven parameters, namely, porosity, thickness of the perforated pipe, diameter of holes, D/d ratio, Mach number, gas temperature, and chamber length and works on double-tuning for cylindrical chamber were done in [9, 10, 11, 12]. Double tuning of elliptical chamber with opposite ends inlet-outlet was carried by kumar [13]. In [13], the double-tuning of elliptical mufflers for variation of different parameters were investigated for offset inlet and outlet pipes. However, the double-tuning of concentric extended inlet/outlet elliptical chamber muffler was done recently by kumar [13]. Elliptical muffler design gives more ground clearance, which is beneficial for vehicles operating on rough terrain or those that require a lower overall height.

Acoustic characteristics of mufflers having elliptical cross-sections was studied by Denia et al. [14]. Effect of the chamber's length as well as the positions of the inlet and exhaust ports were studied. Analytical and numerical study of Denia et al. [14] was corroborated with inlet measurements and excellent agreement between analytical/numerical results and measurements were found. For axially short chamber muffler configurations, the higher-order modes entirely dominate the axial plane-wave mode because the length of the expansion chamber is insufficient to allow the evanescent modes to decay completely. Effect of inlet/outlet port locations on acoustic performance of short elliptical chamber mufflers were done by Selamet and Denia [15] using 3-D FEA. A comparison is made between the impact of the minor and major axes for end outlet port placement.

Limits for condition based on chamber length to major axis length, L/D_1 and inlet/outlet pipe to major axis length was given by Mimani and Munjal [16, 17]. 1-D transverse plane-wave models to analyze axially short-length mufflers with circular and elliptical cross-sections. The 1-D acoustic wave equation was solved in [16] using the matrizant approach, whereas, in [17], the pressure field's analytical solution was derived using the Frobenius solution. It was demonstrated that the transverse plane-wave model could adequately predict the acoustic attenuation characteristics for such short chambers, up to frequencies that are marginally higher than the first higher-order mode's cut-on frequency.

2.1 Motivation and objective of the study

2.1.1 Motivation

Year by year, global energy consumption is getting higher Therefore, the use of fossil fuels is getting higher too. After a few years the world will be run out of conventional energy [18]. There are many applications where fossil fuels are used as a prime source of energy, and IC engine-based vehicles are one of them. These vehicles are run by the use of fossil fuels and after burning these gases affect the environment [19]. Due to these issues, many developments have been made for vehicles based on alternative sources of energy, such as battery-powered vehicles and hydrogen-powered vehicles. Hydrogen power-based vehicles are still in the developing phase. However, such battery-based vehicles are on road which completely operate on battery power source without a internal combustion engine. But in battery-powered vehicles face challenges, such as poor performance in extreme environmental conditions like extremely hot and extremely cold climate, and inadequate charging infrastructure at many places. These limitations have led to the development of hybrid vehicles, which combine battery and IC engine technologies to provide a more versatile solution. Despite their advantages, hybrid vehicles also present some challenges. One significant issue arises when the battery gets considerably discharged which necessitates a switch from battery power to IC engine power. This transition can cause a sudden change in noise levels within the passenger cabin, which in turn disturb the acoustic comfort of passengers. The present study aim at address this issue by developing such efficient mufflers that have wideband noise attenuation characteristic spectrum and higher values of noise attenuation especially at low frequencies. Effective noise attenuation solutions can enhance passenger comfort by minimizing the acoustic impact of switching from electric to IC engine mode, thereby providing a more pleasant and consistent driving experience.

2.1.2 Objectives

Design of exhaust/intake mufflers often subjected to some constraints like, Overall insertion loss(IL) in dBA, Volume of muffler, shape of muffler, length of muffler, and overall backpressure. It is well known that the elliptical muffler configuration are preferred for application in automobiles. The objectives of the present study are given below.

1. Acoustic analysis of compact elliptical cross-section novel muffler configurations for exhaust and intake system of IC engines that have wideband TL spectrum.

2. Synthesis of muffler configuration for different position of inlet/outlet ports.

Chapter 3

3-D FEM analysis of muffler configurations

In this chapter, TL spectra of different elliptical mufflers is computed by 3-D FEA. Furthermore, the effects of the chamber length and the inlet port and outlet port locations on the transmission loss (TL) spectra are examined. In sections 3.1 and 3.2, Acoustic analysis have been done for chamber and elliptical short chamber respectively. Axial plane wave analysis holds for long chamber, whereas transverse plane wave analysis holds for short chambers [17]. The criteria for long chamber and short chamber are given by Eq. 3.1 and Eq. 3.2, respectively.

$$\frac{L}{D_1} \geq 0.5 + 0.5\left(\frac{d}{D_1}\right) \tag{3.1}$$

$$\frac{L}{D_1} \leq 0.25 + 0.25\left(\frac{d}{D_1}\right) \tag{3.2}$$

If the chamber length (L) to major axis length (D_1) ratio does not satisfy inequalities 3.1 and 3.2 then only 3-D analysis can be applied.

3.1 Elliptical long chamber

It can be observed from Fig. 3.1 that effect of double-tuning obtained in extended inlet-outlet muffler as well as concentric tube resonator with perforated bridge between the extended inlet and outlet pipe. The double tuning of extended inlet/outlet pipe was done by incorporating the end-correction. The double-tuning of CTR gets affected due to the inertance of holes as well as the higher-order evanescent waves. Therefore, differential length are incorporated for double-tuning of concentric tube resonator. Extension of the inlet pipe by L/2-$\delta_{0.5L}$ and the outlet pipe by L/2-$\delta_{0.25}$L or vice-versa, lifts the transmission loss spectrum up to k_oL = 4π , where 1^{st}, 2^{nd} and 3^{rd} trough of corresponding troughs of TL spectrum of SEC become peaks of double-tuned mufflers. However, the drawbacks of such chambers include significant back pressure and the production of aerodynamic noise around area discontinuities. These problems can be overcome by inserting a perforated bridge between the extended inlet pipe and extended outlet pipe, and double-tuning of such muffler.

As can be seen in the Fig. 3.1, the TL spectra for the SEC muffler and the effect on the transmission by extending the length of the inlet pipe by L/2 and outlet pipe by L/4 with incorporating the end correction and again providing the perforation bridge between both the extended inlet and outlet pipe. The ratio of the length of the chamber muffler and the major axis length is 3.4. By providing the extension by L/2 and L/4 in inlet and outlet pipe respectively the muffler can lift the three-quarters dips up to the frequency $k_0L = 4\pi$. However, the drawbacks of such chambers include significant back pressure and the production of aerodynamic noise around area discontinuities. Then to remove this problem a perforate bridge are inserting between the extended inlet and extended outlet pipe.

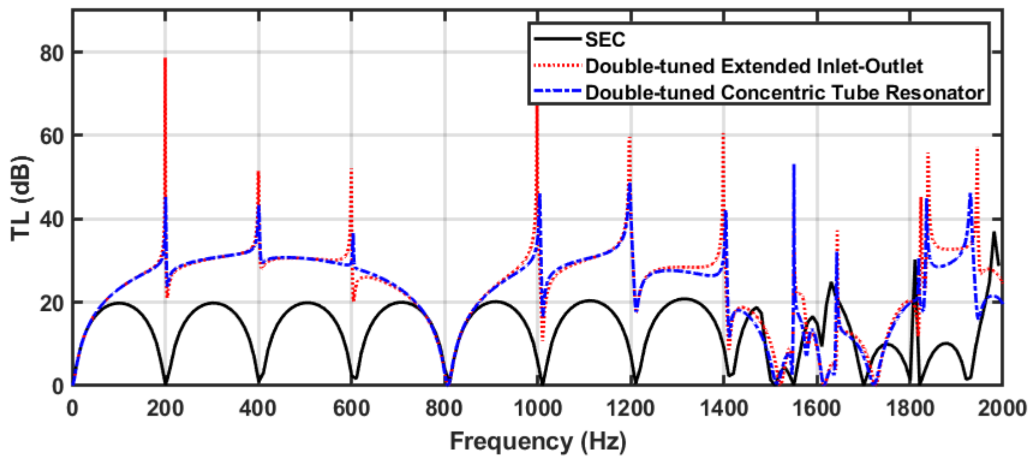

Figure 3.1: Comparison of TL for center inlet center outlet muffler evaluated using 3-D FEM for different muffler configurations, L=3.4 D_1, d = 40 mm and D_1 = 250 mm.

Schematic diagram of a Concentric Tube Resonator muffler is shown in Fig. 3.2. The perforation porosity, hole diameter, and minor axis length are 10%, 3 mm, and 125 mm respectively. Figure 3.3 shows the effect of chamber length on the TL spectrum of double-tuned concentric tube resonator. It can be observed from Fig. 3.3 that the decrement in the muffler length yields wideband TL spectrum. However, wideband TL spectrum is obtained at the cost of less values of TL in low-frequency region. For L/D_1 ratios 3.6, 2.6, and 1.6 and D_1 = 250 mm, the first trough in TL spectrum of DTCTR are at 764 Hz, 1054 Hz, and 1526 Hz, respectively.

The 4^{th} trough of a corresponding SEC is also a trough in case of double-tuned muffler configuration because quarter-wave(Q - W) resonator of acoustic length L/2 surrounding the inlet pipe lifts the troughs at frequencies which are odd multiple of c/2L, and the Q - W resonator of L/4 acoustic length resonator surrounding the outlet pipe lifts the troughs at odd multiple of c/L. Therefore, Q - W resonator of acoustic lengths L/2 and L/4 cannot tune the 4^{th} trough of corresponding SEC. The resonance frequency of Q-W resonator are given by Eq. 3.3.

$$f = \frac{(2n-1)c}{4L_R} \qquad where,\ n = 1,2,3,4,.....\ and\ L_R = \frac{L}{2},\ \frac{L}{4} \tag{3.3}$$

Here, L is the length of the muffler, and c is the sound speed.

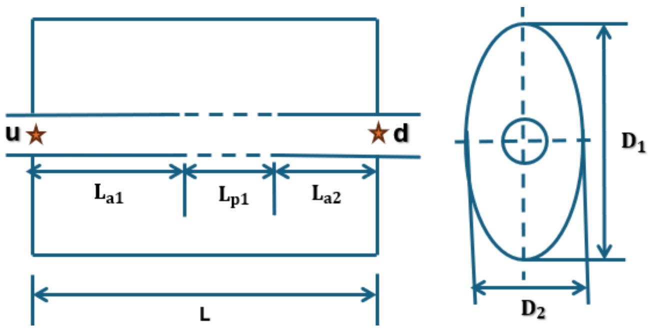

Figure 3.2: Schematic diagram of CTR muffler, L = 1.6 D1.

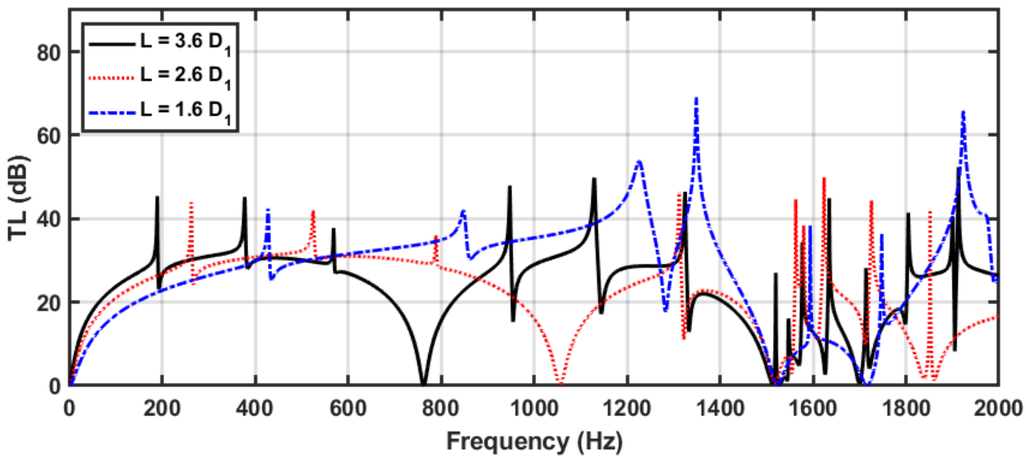

Figure 3.3: Effect of muffler length on TL spectra in CTR muffler

Effect of the port location in the double-tuned muffler with perforated bridge between the extended inlet and outlet pipe is shown in Fig. 3.5 location of the extended inlet pipe and outlet pipe with perforated bridge are shown in Fig. 3.4. Porosity of the perforation, hole diameter, pipe thickness, and minor axis length are 10%, 3 mm, 1.3 mm, and 125 mm respectively. The offset of inlet/outlet pipe on the major axis and on the minor axis are 52.96 mm and

31.96 mm, respectively. It can be observed from the Fig. 3.4 that concentric inlet - outlet and inlet/outlet pipe offset along minor axis have more wideband TL spectrum as compared against the muffler-configuration with inlet/outlet pipe offset along major axis. For brevity, the double-tuned mufflers with offset extended inlet-outlet with perforated bridge and muffler with concentric extended inlet-outlet with perforated bridge are named as DTOTR and DTCTR, respectively.

Figure 3.6 (a, b) show the acoustic pressure field inside the DTOTR muffler configuration with offset along major axis at 611 Hz and 800 Hz, respectively. It can be observed from Fig. 3.6 (a) that the wave propagation is one-dimensional at 611 Hz, and the acoustic pressure in the pipe is much higher as compared against the acoustic pressure in the outlet pipe. Therefore, the TL spectrum one is at 611 Hz. However, at 800 Hz, the acoustic pressure field inside the muffler is three-dimensional where the nodal line appears to be approximately at major axis across the entire length. The amplitude of acoustic pressure are approximately same in the inlet and outlet ports. Therefore, a TL trough is near to 800 Hz.

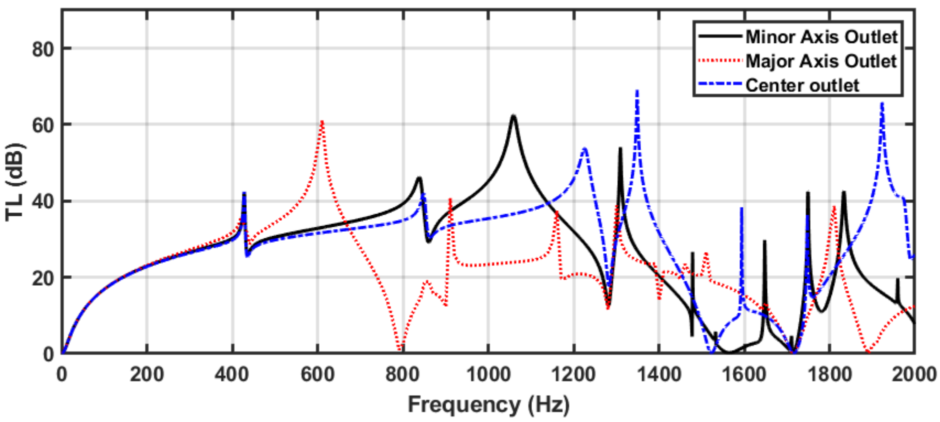

Figure 3.4: Effect of perforated offset bridge between the extended inlet and extended outlet pipe location on TL spectrum for muffler of length, L= 1.6 D_1.

Figure 3.7 shows the schematic diagram of a combination of DTOTR and DTCTR. The DTOTR is the upstream, whereas DTCTR is the downstream. The porosity, hole diameter, perforated pipe thickness, and minor axis length are 10%, 3 mm, 1.3 mm, and 125 mm respectively. The length of the resonators for first muffler L_{a1}, L_{p1} and L_{a2} are $L_a/2$, $L_a/4$ and $L_a/4$ respectively. The length of the resonators for second muffler L_{c1}, L_{p1} and L_{c2} are $L_c/2$, $L_c/4$ and $L_c/4$ respectively.

The side views of combination of a DTOTR and DTOTR /DTCTR muffler with different

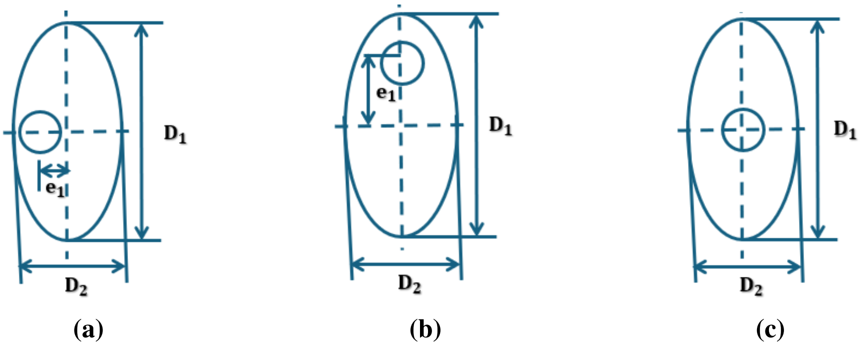

Figure 3.5: Side view of axially long chamber elliptical muffler. (a) Inlet and outlet pipe with perforated bridge are offset along minor axis, (b) Inlet and outlet pipes with perforated bridge are offset along major axis, (c)Inlet and outlet pipes with perforated bridge are offset along center axis

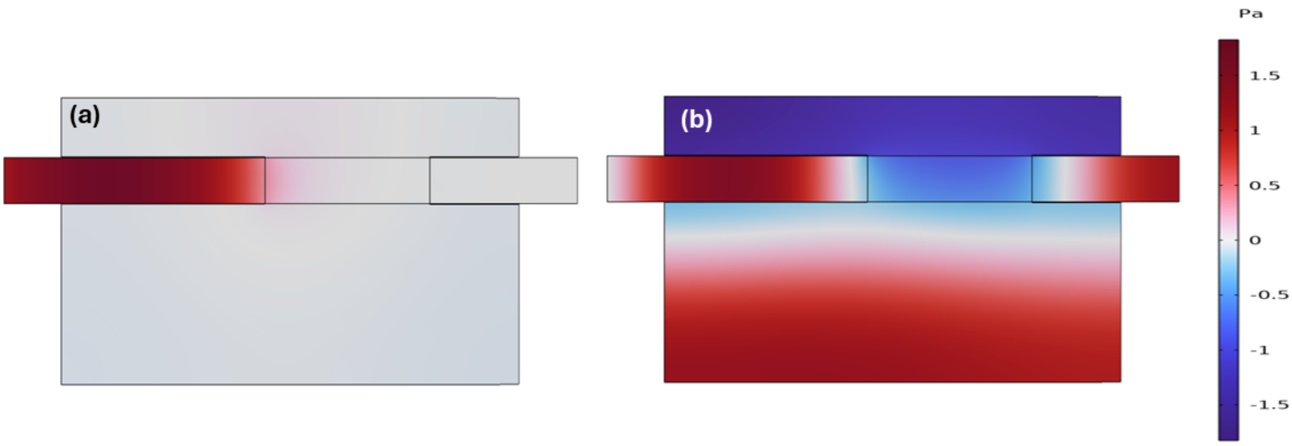

Figure 3.6: Acoustic pressure field inside the DTOTR muffler with offset at major axis.(a) 610 (Hz) and (b) 800 (Hz)

outlet port location are shown in Fig. 3.8. Offset of the outlet port for the second muffler of length (L_c) on the major axis and on the minor axis are 52.96 mm and 31.96 mm, respectively. It can be observed from Fig. 3.9 that the TL spectra of either combination mufflers shown in Fig. 3.7 and 3.8 are shown in Fig. 3.9, if the outlet port of the second muffler (L_c) is either placed at the center or at minor axis results wideband TL spectrum as well as higher values of TL as compared against the muffler configuration with both inlet and outlet, are offset at major axis.

The dual chamber perforated muffler configuration with side view shown in Fig. 3.8 each chamber are not double-tuned because the inlet and outlet pipes are not inline. Due to the inlet and outlet ports (not inline) the Q - W resonator of lengths L_{a2} and L_{c1} cannot be tuned. Moreover for the inlet port and outlet port not being inline, such muffler configurations are

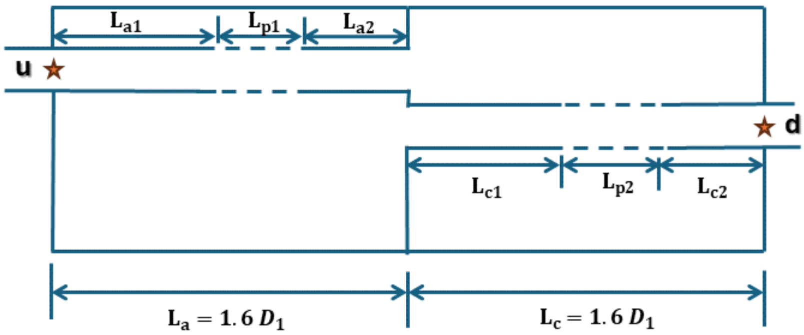

Figure 3.7: Schematic diagram of the combination of one offset tube resonator and one concentric tube resonator with inlet port is offset (e = 52.96 mm) along the major axis and the outlet port is at centre, L_a = L_c = 1.6 D1.

multiply connected muffler configuration.

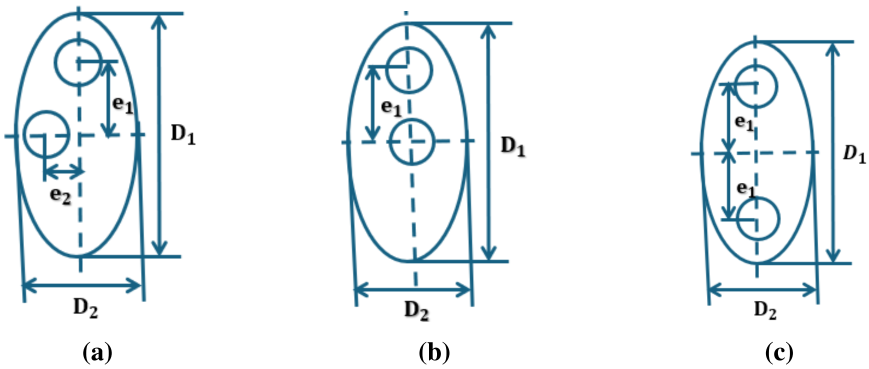

Figure 3.8: Side views of combination of two elliptical DTOTR/DTCTR. (a) Inlet is offset at major axis and outlet is offset at minor axis, (b) Inlet is offset at major axis and center outlet, (c) Inlet and outlet are offset at major axis on two sides.

It can be observed from Fig. 3.9 that if both the perforated inlet pipe and outlet pipe are offset along the major axis then TL values at most frequencies are less than those compared with the muffler configuration with outlet pipe either offset along the minor axis or at center. The higher order mode with nodal line on major axis gets cut - on due to the offset of inlet/outlet pipe with perforated bridge along major axis. However the cut - on of higher order mode gets nullified if the outlet in the second chamber is on minor axis. This is the reason for variation in TL spectra plotted in Fig. 3.9 for muffler configuration shown in Fig. 3.8.

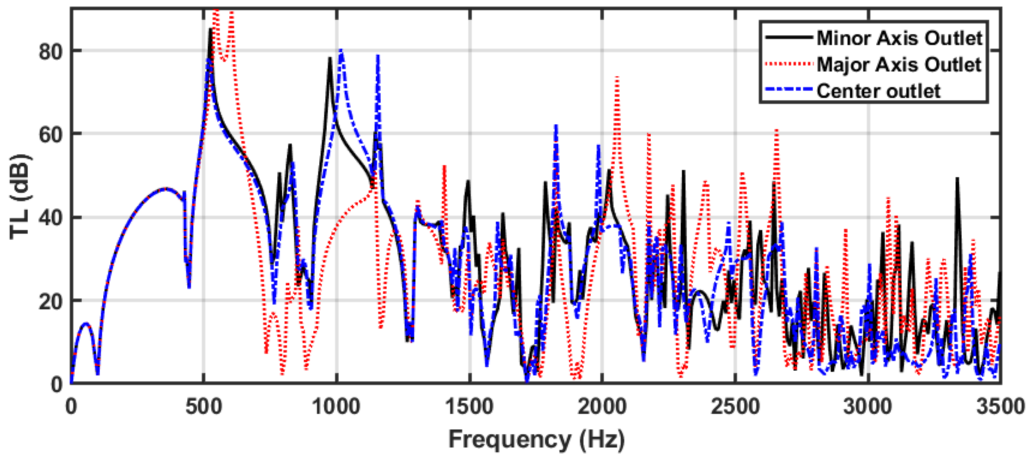

Figure 3.9: Effect of outlet port location on TL spectrum of the combination muffler shown in Figs. 3.7 and 3.8.

Figure 3.10 shows the schematic diagram of a combination of DTCTR. The upstream and downstream are at center. The porosity, hole diameter, perforated pipe thickness, and minor axis length are 10%, 3 mm, 1.3 mm, and 125 mm respectively. The length of the resonators for first muffler L_{a1}, L_{p1}, and L_{a2} are $L_a/2$, $L_a/4$, and $L_a/4$ respectively. The length of the resonators for second muffler L_{c1}, L_{p1}, and L_{c2} are $L_c/2$, $L_c/4$, and $L_c/4$ respectively.

The side views of combination of a DTOTR and DTOTR /DTCTR muffler with different outlet port location are shown in Fig. 3.11. It can be observe from Fig. 3.12 that the TL spectra of either combination mufflers shown in Fig. 3.10 and 3.11 are shown in Fig. 3.12, if the inlet - outlet port of muffler is either placed at the center or at minor axis results wideband TL spectrum as well as higher values of TL as compared against the muffler configuration with both inlet and outlet, are offset at major axis.

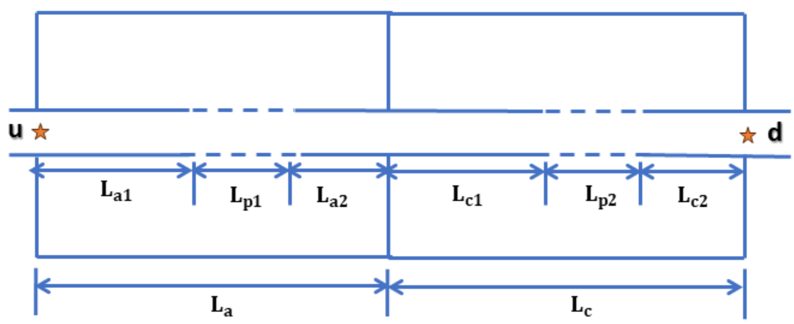

Figure 3.10: Schematic diagram of double concentric tube resonator with center inlet - outlet pipes, L_a = L_c = 1.6 D1.

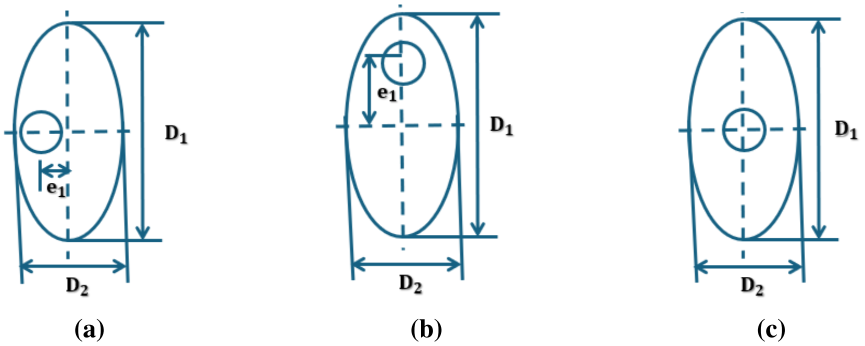

Figure 3.11: Side view of axially long chamber elliptical muffler. (a) Inlet and outlet pipe with perforated bridge are offset along minor axis, (b) Inlet and outlet pipes with perforated bridge are offset along major axis, (c)Inlet and outlet pipes with perforated bridge are offset along center axis

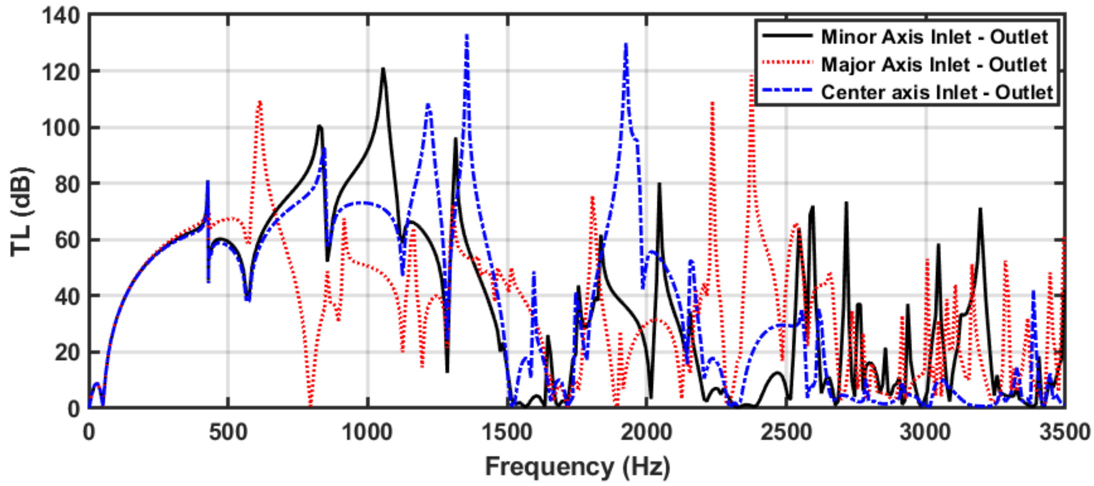

Figure 3.12: Effect of outlet port location on TL spectrum of the combination muffler shown in Figs. 3.10 and 3.11.

3.2 Elliptical short chamber

Figure 3.13 shows the schematic diagram of a short chamber muffler with the inlet port at the major axis and the outlet port at the center. For such short chamber mufflers, the plane wave propagation is along transverse direction of the elliptical chamber. This short chamber muffler has two resonators along with the main line. The length of the short chamber mufflers is (L_b = 0.2 D_1). The length of major axis diameter (D_1) and the minor axis diameter (D_2) are 250 mm and 125 mm, respectively. Theefore, the variable area duct region above the inlet port and below the outlet port, the resonator are placed as shunt element in electroacoustic circuit for plane wave analysis discuss in the next chapter.

Figure 3.14 shows the side views of the elliptical short chamber mufflers with different port

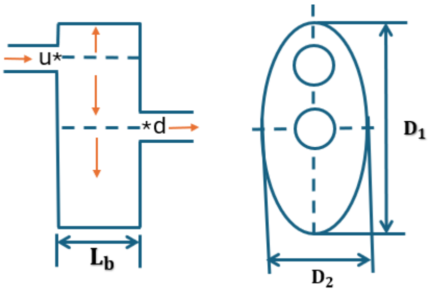

Figure 3.13: Short chamber elliptical muffler, with offset inlet along major axis and centre outlet.

locations, offsets of the ports on the major axis and on the minor axis are 52.96 mm and 31.96 mm, respectively.

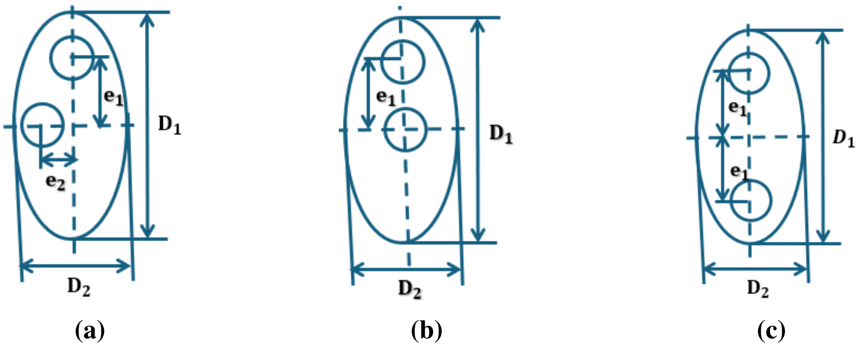

Figure 3.14: Side views of the elliptical short chamber mufflers. (a) Major axis inlet and center outlet, (b) Schematic diagram of short chamber muffler with major axis inlet and minor axis outlet.

Eigenvalue problem in 2-D plane wave showed numerically by finite element method, the transverse mode shapes and cut-on frequencies of higher-order modes of elliptical cross-section are shown in Fig. 3.15. By using the modal analysis, Mimani and Munjal [20] suggested the placements of the -ports on these zero-pressure lines which helps to extend the limit for the plane wave analysis and the TL spectrum becomes wideband if ports are located judiciously as shown in Fig. 3.16.

It can be observed from Fig. 3.16 that wideband TL if center of inlet is placed at major axis on the nodal lines of $(3, 1)_e$ mode and the outlet is placed on the minor axis the wideband TL spectrum is achieved till the cut-on of $(4, 1)_e$ mode. If the inlet port and the outlet port are placed at the nodal line of $(3, 1)_e$ mode then $(1, 1)_e$ mode and $(3, 1)_e$ mode gets exited. The acoustic pressure amplitudes at the inlet and outlet port same. Therefore, TL troughs are observed at frequencies corresponding to the cut-on of $(1, 1)_e$ mode and $(3, 1)_e$ mode. For muffler configuration with the inlet and outlet ports offset along major axis.

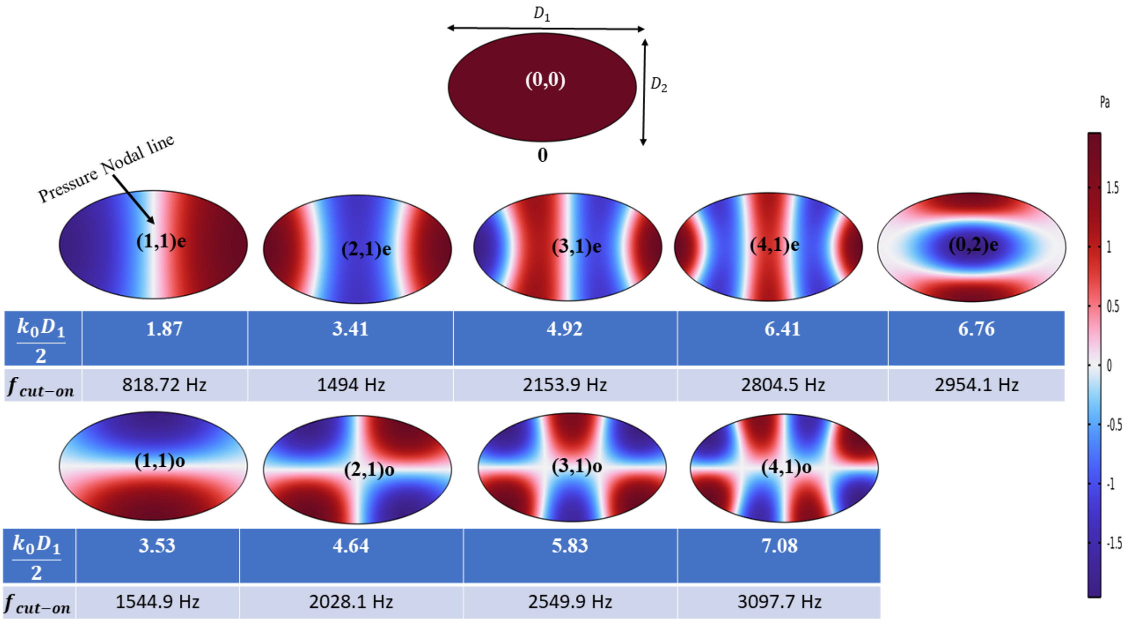

Figure 3.15: Mode shapes of elliptical cross-section [20].

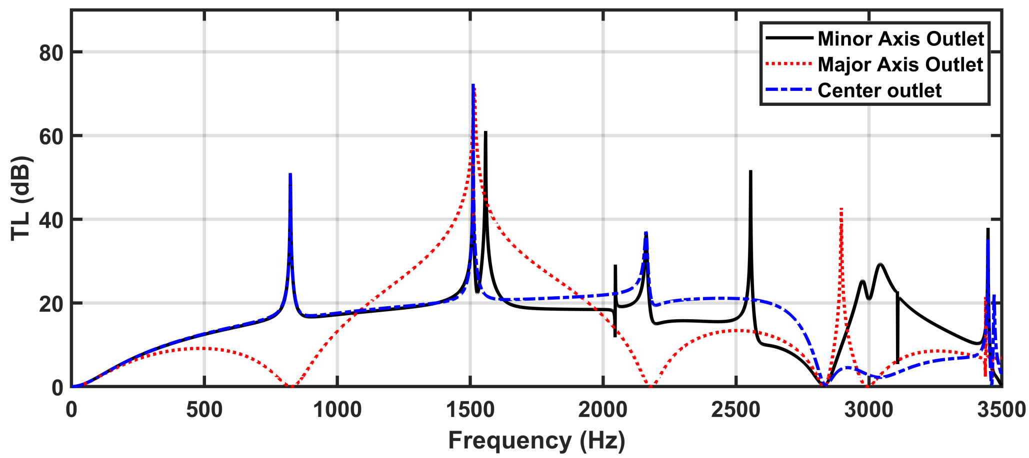

Figure 3.16: Effect of port locations on 3-D FEM computed TL spectra for mufflers with length, L_b = 0.2 D_1 [20].

Chapter 4

Synthesis of Muffler Configurations

It is well known that the plane wave analysis is less time consuming as compared against the 3-D FEM. In general, the plane wave analysis of mufflers holds right up to the cut-on of first possible higher order modes. Plane wave analysis for cascaded-element mufflers and multiply-connected element mufflers are done by transfer matrix methode (TMM) [4] and integrated transfer matrix (ITM) approach [4, 21], respectively. The 1-D TMM and 1-D ITM approach are applied for synthesis of muffler configurations, because these methods do faster computation till the cut-on of first possible higher order mode. Fortunately, for medium size muffler configurations, the unmuffled SPL spectra of the exhaust system and intake system, therefore, the insertion loss spectrum of the mufflers are more significant up to the cut-on of first possible higher order mode. Mufflers are first analyzed by the 1-D TMM or 1-D ITM approach due to its faster computation. However, the 3-D FEM used to validate the 1-D analysis up to the first possible higher order mode cut-on and the analysis of muffler configurations beyond the plane wave limit.

In the present study, the novel muffler configurations are basically combination of elliptical long DTOTR/DTCTR and elliptical short chamber mufflers with different port locations. Therefore, in section 4.1, derivation of the transfer matrices of double-tuned muffler with perforated bridge between the extended inlet pipe and extended outlet pipe, and elliptical short chamber muffler are presented. Later, the application of the transfer matrices of these muffler configurations are used to find out the transfer matrix of different combination mufflers. At the end, the comparison of TL spectra of different muffler configurations computed by 1-D TMM and 3-D FEM are done which leads to the synthesis of novel muffler configurations analyzed in the present study.

4.1 Transfer Matrix Method (TMM)

4.1.1 Transfer Matrix for the OTR/CTR

Schematic diagram of a concentric tube resonator (CTR) with extended inlet and extended outlet is shown in Fig. 4.1. For axially long chambers, the plane wave analysis of CTR and OTR would be same. Therefore, the transfer matrix relating the acoustic state variables at upstream and downstream of an OTR or a CTR is same. In this section, the plane wave analysis is done using 1-D transfer matrix method (TMM). The TMM needs the muffler representation as a cascade of elements [4]. It is shown in Fig. 4.1 that the muffler is divided as cascade of three elements. Here, element 2 consists of two regions: 2p (for perforated pipe) and 2a (for annular region surrounding the perforated pipe). Derivation of the transfer matrix relating the acoustic state variables at the upstream of perforated segment to that of the downstream involves the Q-W resonator impedances surrounding the extended inlet/outlet pipes. The details are discussed here.

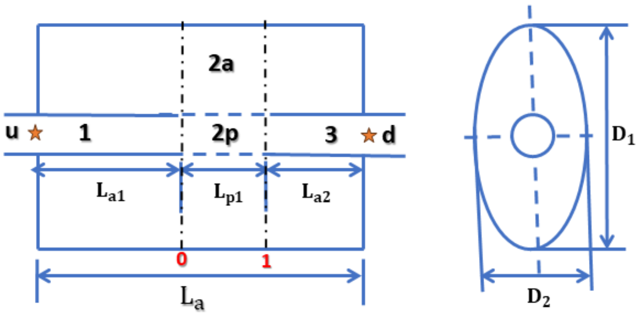

Figure 4.1: Schematic diagram of an extended perforated pipe muffler, L = 1.6 D_1.

The relation between the acoustic state variables of perforated pipe and annular region surrounding the perforated pipe at the upstream of perforate is given by Eq. 4.1

$$\begin{bmatrix} p_{2a,0} \\ v_{2a,0} \\ p_{2p,1} \\ v_{2p,1} \end{bmatrix} = \left[E_{2a,2p,0-1}\right]_{4\times4} \begin{bmatrix} p_{2a,1} \\ v_{2a,1} \\ p_{2p,1} \\ v_{2p,1} \end{bmatrix} \tag{4.1}$$

Here, subscripts '2a' and '2p' stand for the annular region surrounding the perforated pipe and the perforated pipe, respectively. $E_{2a,2p,0-1}$ represents the 4*4 transfer matrix which relates the acoustic state variables of domain '2a' and '2p' between section 0 and section 1 as shown in Fig. 4.1.

The impedance of Q-W resonator at the upstream and downstream of perforate are expressed by Eq. 4.2 and 4.3.

$$Z_U = \frac{p_{2a,0}}{-v_{2a,0}} = (-jY_0 cotk_0 L_{a1}) \tag{4.2}$$

$$Z_D = \frac{p_{2a,1}}{v_{2a,1}} = -jY_0 cotk_0 L_{a2} \tag{4.3}$$

Equation 4.1, 4.2 and 4.3 can be written in the following matrix form as Eq. 4.4.

$$\underbrace{\begin{bmatrix} \multicolumn{4}{c}{} & 0 & 0 \\ \multicolumn{4}{c}{[E_{2a,2p,0-1}]^{-1}} & 0 & 0 \\ \multicolumn{4}{c}{} & -1 & 0 \\ \multicolumn{4}{c}{} & 0 & -1 \\ 1 & Z_U & 0 & 0 & 0 & 0 \\ 0 & 0 & 0 & 0 & -1 & Z_D \end{bmatrix}}_{[A]} \begin{bmatrix} p_{2a,0} \\ v_{2a,0} \\ p_{2p,1} \\ v_{2p,1} \\ p_{2a,1} \\ v_{2a,1} \end{bmatrix} = \begin{bmatrix} 0 \\ 0 \\ p_{2p,1} \\ v_{2p,1} \\ 0 \\ 0 \end{bmatrix} \tag{4.4}$$

Inverse of matrix A is named matrix B. To do the plane wave analysis we need the transfer matrix which relates the acoustic state variables at the upstream and downstream of perforated pipe. This transfer matrix is given by Eq. 4.5, using Eq. 4.4

$$\begin{bmatrix} p_{2p,0} \\ v_{2p,0} \end{bmatrix} = \begin{bmatrix} B_{33} & B_{34} \\ B_{43} & B_{44} \end{bmatrix} \begin{bmatrix} p_{2p,1} \\ v_{2p,1} \end{bmatrix} \tag{4.5}$$

Electro-acoustic circuit diagram for the CTR or a similar OTR is shown in Fig. 4.2

Transfer matrix which relates the acoustic state variables at the upstream of the muffler proper to these at the downstream of the muffler proper is given by Eq. 4.5.

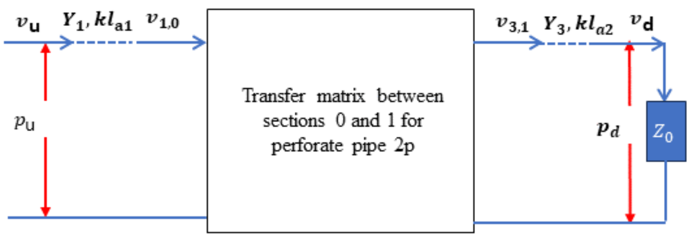

Figure 4.2: Electro-acoustic circuit daigram of a CTR or an OTR with the extended inlet pipe and outlet pipe.

$$\begin{bmatrix} p_{u,MP} \\ v_{u,MP} \end{bmatrix} = \underbrace{\begin{bmatrix} cos(k_0L_{a1}) & jY sin(k_0L_{a1}) \\ \frac{j}{Y_1} sin(k_0L_{a1}) & cos(k_0L_{a1}) \end{bmatrix} \begin{bmatrix} B_{33} & B_{34} \\ B_{43} & B_{44} \end{bmatrix} \begin{bmatrix} cos(k_0L_{a2}) & jY sin(k_0L_{a2}) \\ \frac{j}{Y_2} sin(k_0L_{a2}) & cos(k_0L_{a2}) \end{bmatrix}}_{T_{OTR/CTR}} \begin{bmatrix} p_{d,MP} \\ v_{d,MP} \end{bmatrix} \tag{4.6}$$

Here, subscripts 'MP', 'u', and 'd' stand for the muffler proper, upstream and downstream, respectively. Y_1 and Y_2 are characteristic impedances of the inlet pipe and outlet pipe, respectively.

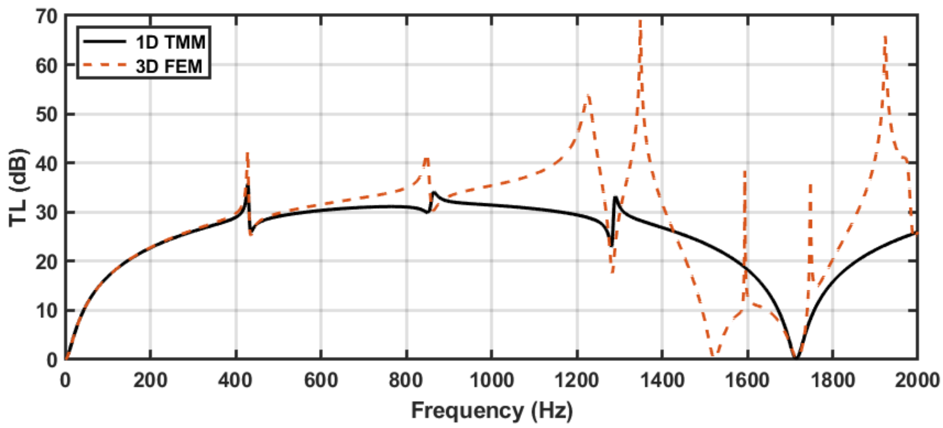

Figure 4.3: Comparison of TL evaluated using 1-D TMM and 3-D FEM for CTR.

Figure 4.3 shows the TL spectra computed by 1-D TMM and 3-D FEM for CTR muffler. It can be observed from Fig. 4.3 that the TL spectra computed by 1-D TMM and 3-D FEM are exactly matching up to the frequency of 448 Hz after that the deviation takes place in both the spectra. Here, the reason of the deviation in the 1-D TMM and 3-D FEM are shown in Fig. 4.4.

Figure 4.4 shows the acoustic pressure variation for frequencies 450 Hz and 560 Hz at three

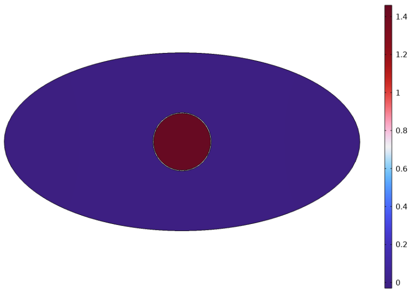

(a)

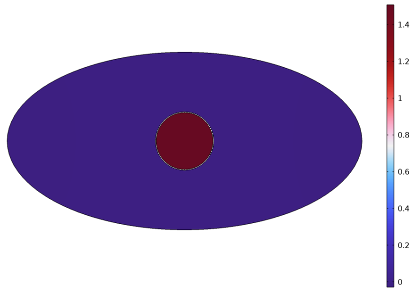

(d)

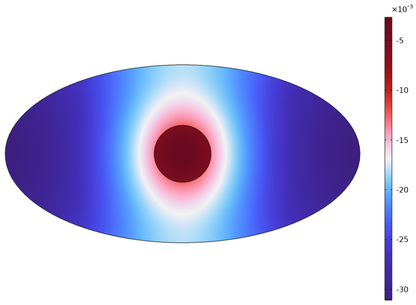

(b)

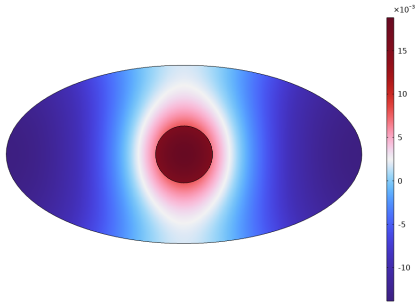

(e)

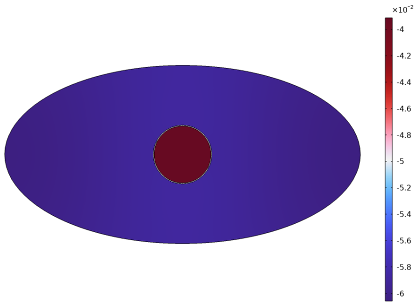

(c)

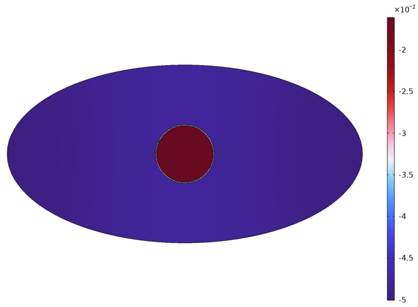

(f)

Figure 4.4: Acoustic pressure field inside the DTCTR muffler at three different planes. Parts a-c shows the acoustic pressure field variation at 450 Hz, while parts d-f shows the acoustic pressure field variation at 560 Hz.

different planes (first plane is taken at 100 mm distance from the chamber start, second plane is taken at 250 mm from the chamber start, and the third plane is taken from the 350 mm from the chamber start.) in the DTCTR. Figure 4.4a to 4.4c shows the acoustic pressure field variation at 450 Hz, here in Figs 4.4a and 4.4c (For cut plane 1 and cut plane 3) the acoustic pressure is same into the pipe and the annular region but in the Fig 4.4b the acoustic pressure is different in to the annular region. Similarly the Fig. 4.4d to 4.4f shows the acoustic pressure field variation at 560 Hz, here in Figs 4.4d and 4.4f (For cut plane 1 and cut plane 3) the acoustic pressure is same into the pipe and the annular region but in the Fig 4.4e the acoustic pressure is different in to the annular region. So, because of this pressure variation inside the DTCTR muffler the plane wave analysis (1-D TMM) are showing the deviation as compare to the 3-D FEM analysis.

4.1.2 Transfer Matrix for the short chamber muffler

Transverse plane wave analysis is the reasonable approximation for wave propagation in a short elliptical chamber [16]. Schematic diagram of a short elliptical chamber with the inlet port offset along major axis and the outlet port is at centre, and the inlet port offset along major axis and the outlet port is offset along the minor axis are shown in Fig. 4.5 (a) and 4.5 (b), respectively. From the transverse plane wave analysis point of view, both muffler configurations are same. The electro-acoustic circuit diagram of the short elliptical chambers is shown in Fig. 4.6.

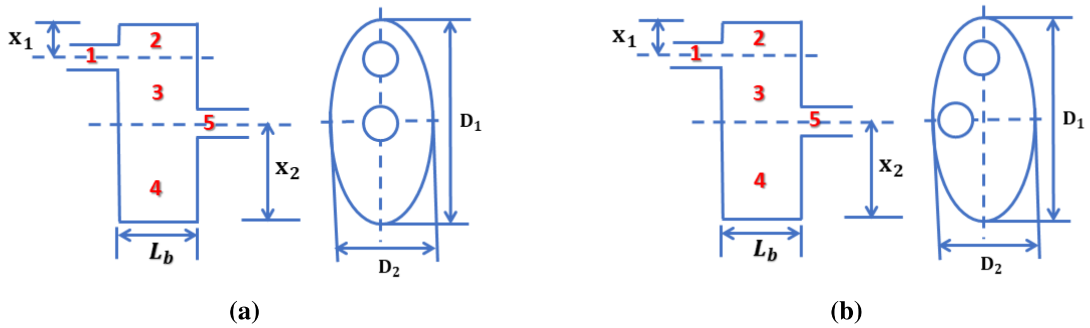

Figure 4.5: Schematic diagram of short chamber muffler. (a) Major axis inlet and center outlet, (b) Major axis inlet and minor axis outlet.

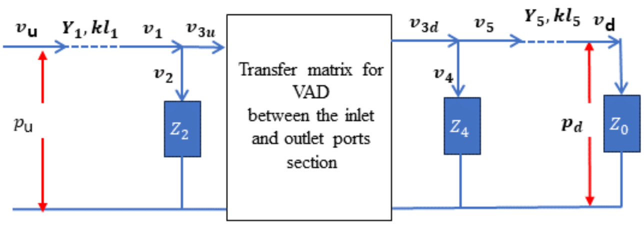

Figure 4.6: Electro-acoustic circuit diagram of a short chamber muffler.

Z_2 and Z_4 are impedance expressions of these variable area closed end quarter wave resonator cavity as shown in Fig. 4.5. Now the impedance expression are given in Eq. 4.7 and Eq. 4.8, where, the $F_1(y)$ and $F_2(y)$ are frobenius polynomial function. The value of y_1 and y_2 can be calculated by the formula, $y_1 = \frac{x_1}{D_1}$ and $y_2 = \frac{x_2}{D1}$. Where x_1 and x_2 are the distances for the inlet and the outlet pipe from the top and the bottom of the muffler, and D_1 is the major axis diameter.

$$Z_2 = j\beta \frac{F_1(y_1)}{F_1'(y_1)} \tag{4.7}$$

$$Z_4 = j\beta \frac{F_1(y_2)}{F_1'(y_2)} \tag{4.8}$$

The transfer matrix which relates the acoustic state variables at upstream of the muffler proper to these at the downstream of muffler proper is given by Eq. 4.9.

$$\begin{bmatrix} p_{u,MP} \\ v_{u,MP} \end{bmatrix} = \underbrace{\begin{bmatrix} 1 & 0 \\ \frac{1}{Z_2} & 1 \end{bmatrix} \begin{bmatrix} TM_{VAD} \end{bmatrix} \begin{bmatrix} 1 & 0 \\ \frac{1}{Z_4} & 1 \end{bmatrix}}_{B} \begin{bmatrix} p_{d,MP} \\ v_{d,MP} \end{bmatrix} \tag{4.9}$$

Figure 4.7 shows the comparison of TL spectra for the short chamber muffler which are computed by the plane wave analysis (1-D TMM) and 3-D FEM analysis. The TL spectra from the 1-D TMM are exactly same up to the 843 Hz after that the deviation in both the spectra are take place. The reason of this deviation is because the acoustic pressure variation inside this short chamber are same at every cut planes up to the frequency 843 Hz, after that the pressure variation at each cut planes are start changing that is why the plane wave analysis (1-D TMM) is are not holding the actual performance.

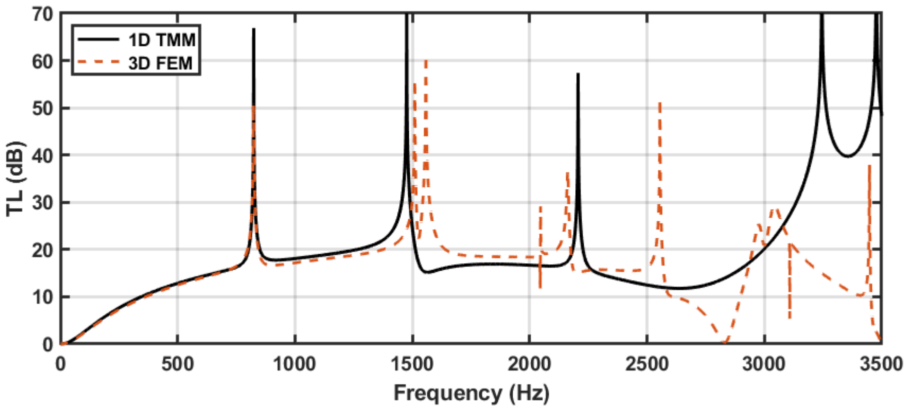

Figure 4.7: Comparison of TL evaluated using 1-D TMM and 3-D FEM for short chamber muffler.

4.2 Combination muffler

The broadband TL spectrum is obtained for small length of the chamber in the plane wave region, the double-tuned muffler configuration with perforated elements has more TL value in the low-frequency region as compared with the short elliptical chamber, but in a narrow frequency band. In this section, to have the advantage of both mufflers, the performance of the combination muffler is analyzed using the one-dimensional Transfer Matrix Method (1-D TMM). This combination muffler consists of an axially-short chamber which is placed in between the two axially-long double-tuned perforated element mufflers.

Fig. 4.8 represents the schematic diagram of the design muffler configurations which consists of two long chamber mufflers and a short chamber muffler in between these long chamber mufflers. The inlet pipe of this combination muffler is offset along the major axis whereas the outlet pipe is at the center. The overall transfer matrix which correlates the inlet state variables to the outlet state variables of a combination muffler can be obtained by multiplying the transfer matrix of each chamber. The electro-acoustic analogy of a combination muffler are shown in the Fig. 4.9.

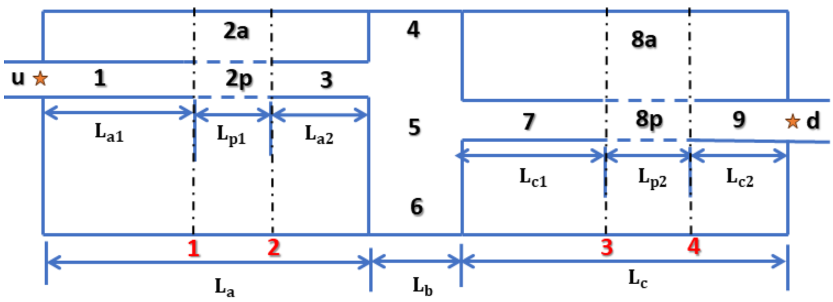

Figure 4.8: Schematic diagram of a combination muffler.

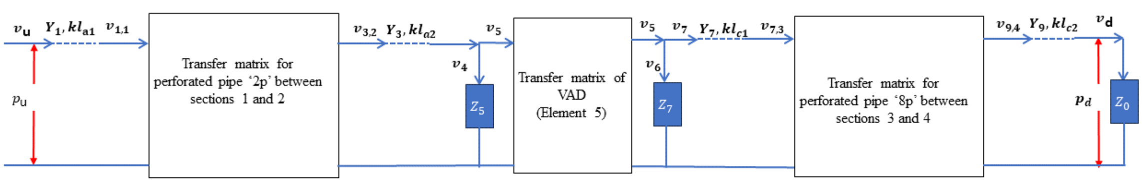

Figure 4.9: Electro-acoustic analogy of a combination muffler.

Now Eq. 4.7 gives the relation between the inlet state variables to the outlet state variables for a long chamber muffler, and Eq. 4.9 gives the relation between the inlet state variables to the outlet state variables for a short chamber muffler. Now Eq. 4.10 gives the relation between the upstream and the downstream of the designed combination muffler. This relation is applicable to all the design configurations.

$$\begin{bmatrix} p_u \\ v_u \end{bmatrix} = \begin{bmatrix} A \end{bmatrix} \begin{bmatrix} B \end{bmatrix} \begin{bmatrix} A \end{bmatrix} \begin{bmatrix} p_d \\ v_d \end{bmatrix} \tag{4.10}$$

So, after analyzing all the variations of length and port location in the extended perforated tube muffler and in the short chamber muffler, four different types of combination muffler are introduced. Figure 4.10 shows configuration 1 (a) which has two long chamber mufflers with equal in length and are placed on both side of the muffler and the short chamber is placed at the center of both the long chamber mufflers. The configuration 1 (b) have same dimension but the outlet port location are different as shown in Fig. 4.11.

Figure 4.12 shows configuration 2 (a) which has two long chamber mufflers, the first long chamber muffler length is $1.4D_1$ and the second long chamber muffler length is $1.8D_1$. The first long chamber muffler are placed at the inlet side and the second long chamber are placed at the outlet side and the short chamber muffler are placed at the center of both the long chamber muffler. Configuration 2 (b) has the same dimension but the outlet port locations are different as shown in Fig. 4.13. the detailed dimensions of the designed muffler configurations are given in Table 4.1.

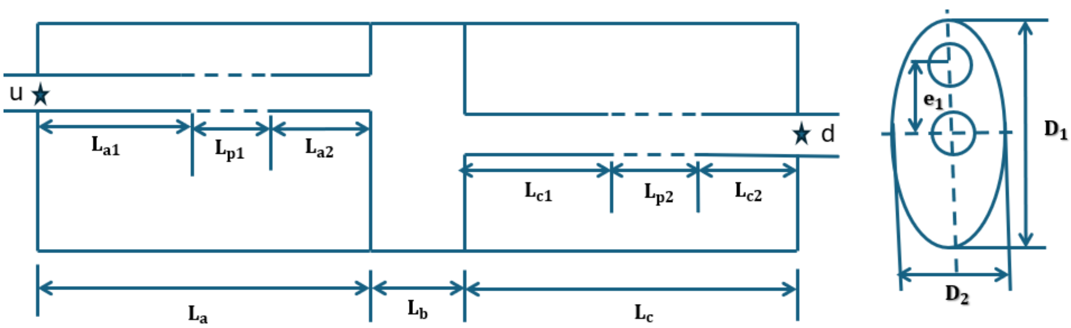

Figure 4.10: Schematic of configuration 1(a) with inlet port is offset along the major axis and outlet port is at the center.

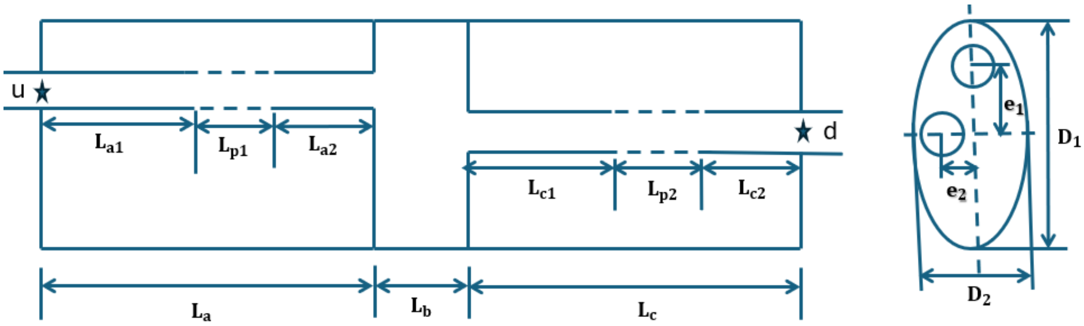

Figure 4.11: Schematic of configuration 1(b) with inlet and outlet port is offset along major and minor axis respectively.

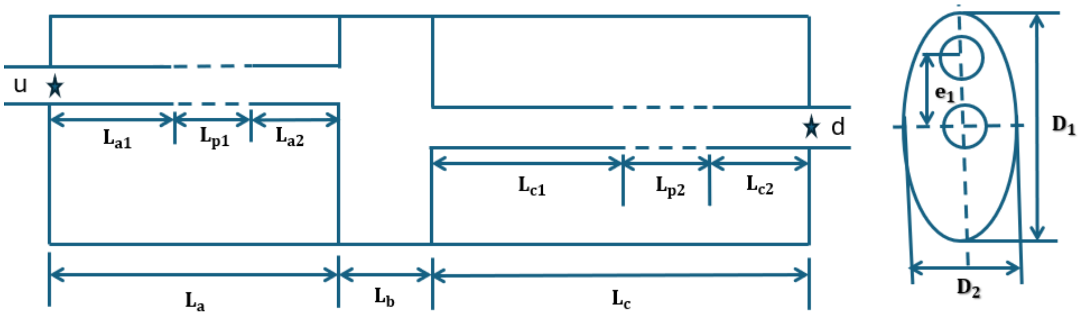

Figure 4.12: Schematic of configuration 2(a) with inlet port is offset along the major axis and outlet port is at the center.

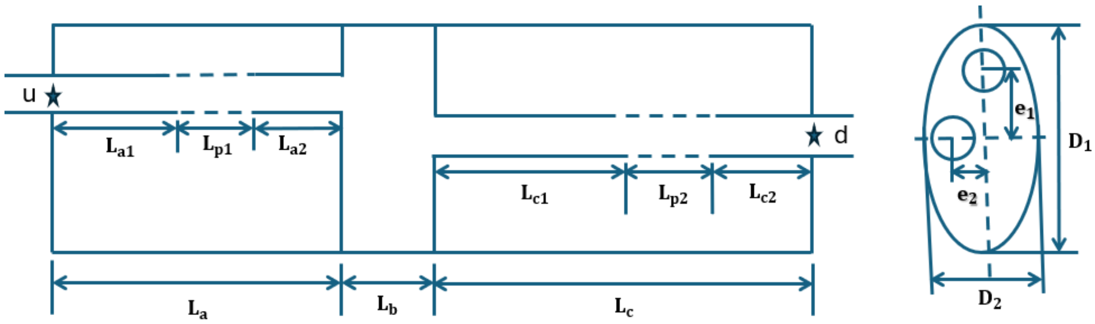

Figure 4.13: Schematic of configuration 2(b) with inlet and outlet port is offset along major and minor axis respectively.

Figure 4.14 demonstrates the comparison of transmission loss curves calculated between analytical and numerical results for configuration 1(a). The plotting is done up to a frequency range of 0–3500 Hz. The cut-on frequency for configuration 1 (a) is 816 Hz. The first peak are coming at 428 Hz because of the $L_(a1)$ resonator. The transmission loss spectra from the 1-D TMM and 3-D FEM after tuning were found to be exactly the same up to the first peak (428.27 Hz) after that both spectra were close to each other up to the 2600 Hz. The maximum value of TL is 110 dB which is coming near 611 Hz from the 3-D FEM analysis.

Table 4.1: Geometrical parameters for different muffler configurations

Parameters	**Configuration 1**	**Configuration 2**
Length of major axis, D_1 (mm)	250	250
length of minor axis, D_2 (mm)	125	125
Diameter of inlet/outlet pipe, d (mm)	40	40
Length of 1^{st} long chamber, L_a (mm)	1.6 D_1	1.4 D_1
Length of short chamber, L_b (mm)	0.2 D_1	0.2 D_1
Length of 2^{nd} long chamber, L_c (mm)	1.6 D_1	1.8 D_1
Porosity, ϕ	10%	10%
Diameter of hole, d_h (mm)	3	3
Pipe wall thickness, t_h (mm)	1.3	1.3
Offset along major axis, e_1 (mm)	52.96	52.96
Offset along minor axis, e_2 (mm)	31.96	31.96

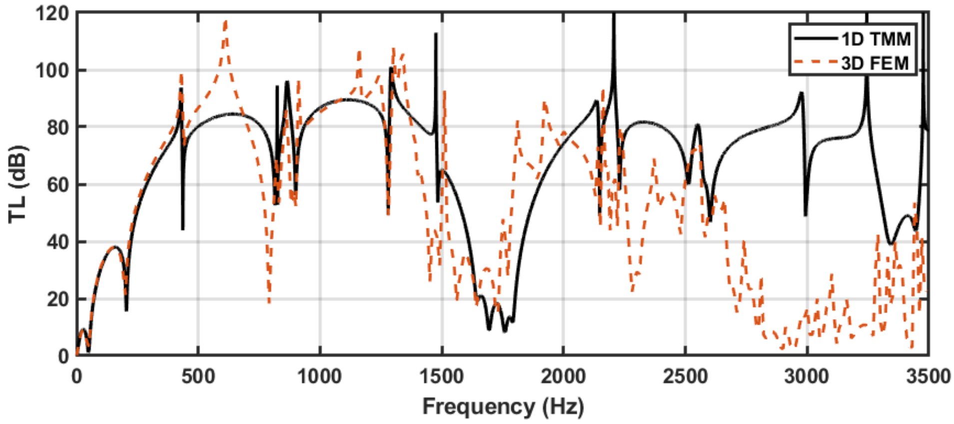

Figure 4.14: Comparison of TL evaluated using 1-D TMM and 3-D FEM for configuration 1(a).

Figure 4.15 demonstrates the comparison of transmission loss curves calculated between analytically and numerically for the configuration 1(b). Here the dimensions of configuration 1 (b) are exactly the same as configuration 1 (a) the only difference is there is that the outlet port locations are different. The plotting is done up to a frequency range of 0–3500 Hz. The cut-on frequency for the configuration 1 (b) is 816 Hz. The first peak are coming at 428 Hz because of the L_{a1} resonator. The transmission loss spectra from the 1-D TMM and 3-D FEM after tuning were found to be exactly the same up to the first peak (428.27 Hz) after that both spectra were close to each other up to the 2600 Hz. The maximum value of TL is 110 dB which is coming near 611 Hz from the 3-D FEM analysis.

Though both the mufflers have same dimension that is why the first peak and the cut on frequency are same, for both the muffler.

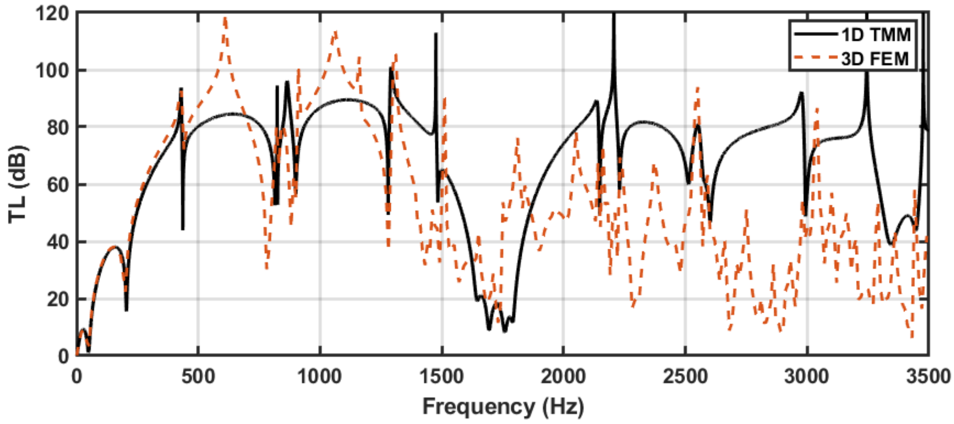

Figure 4.15: Comparison of TL evaluated using 1-D TMM and 3-D FEM for configuration 1(b).

Figure 4.16 demonstrates the comparison of transmission loss curves calculated between analytical and numerical analysis for configuration 2(a). Configuration 2(a) has two different lengths of eccentric extended perforated tube muffler with the short chamber muffler. The plot is taken up to a frequency range of 0 to 3500 Hz. The cut-on frequency for the configuration 1 (b) is 816 Hz. In the TL spectra two peaks are coming in between the 500 Hz frequency, The first peak (381.27 Hz) is coming because of the extended pipe resonator $L_{c1}/2$ and the second peak (490 Hz) is coming because of the extended pipe resonator $L_{a1}/2$.

The transmission loss spectra from the 1-D TMM and 3-D FEM after tuning were found to be exactly the same up to the first peak (381.27 Hz) after that both spectra were close to each other up to the 2600 Hz. The maximum value of TL is 110 dB which is coming near 600 Hz from the 3-D FEM analysis.

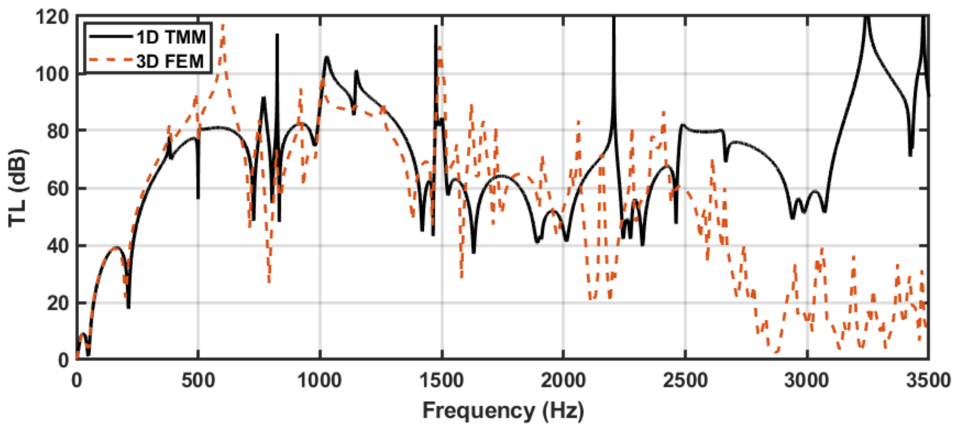

Figure 4.16: Comparison of TL evaluated using 1-D TMM and 3-D FEM for configuration 2(a).

Figure 4.17 shows the comparison of transmission loss curves calculated between analytical and numerical analysis for configuration 2(b). Here the dimensions of configuration 2 (b) are exactly the same as configuration 2 (a) the only difference is there is that the outlet port locations are different from configuration 2 (a). The transmission loss spectra from the 1-D TMM and 3-D FEM after tuning were found to be exactly the same up to the first peak (381.27 Hz) after that both spectra were close to each other up to the 2460 Hz. The maximum value of TL is 100 dB which is coming near 600 Hz from the 3-D FEM analysis.

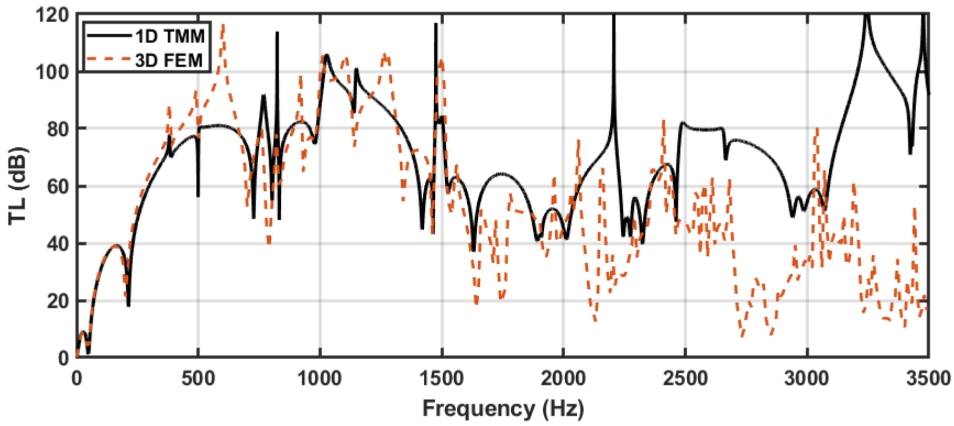

Figure 4.17: Comparison of TL evaluated using 1-D TMM and 3-D FEM for configuration 2(b).

4.3 Comparision of TL spectra for combination mufflers

In this section, the TL spectra from the 3-D FEM for the combination muffler are compared. Figure 4.18 shows the comparison of transmission loss spectra from the numerical analysis for Configuration 1(a) and Configuration 1(b). Both the configurations gave the same transmission loss up to 930 Hz, after that both were very close to each other and followed the same trend but after 2600 Hz, a small variation was there in both spectra.

From Fig. 4.18 the highest TL value for configuration 1 (a) and configuration 1 (b) is 110 dB at 611 Hz and subsequently the trough is coming up to 30 dB at the 781 Hz. The reason for the highest TL value can be seen in Fig. 4.19(a) that, the impedance for the frequency 611 Hz is very small and the total acoustic pressure at the outlet of the muffler configuration is zero. The reason for the trough in the TL at 781 Hz can be seen in Fig. 4.19(a) that, the impedance for the frequency 781 Hz are high and the total acoustic pressure at the outlet of the muffler configuration is high.

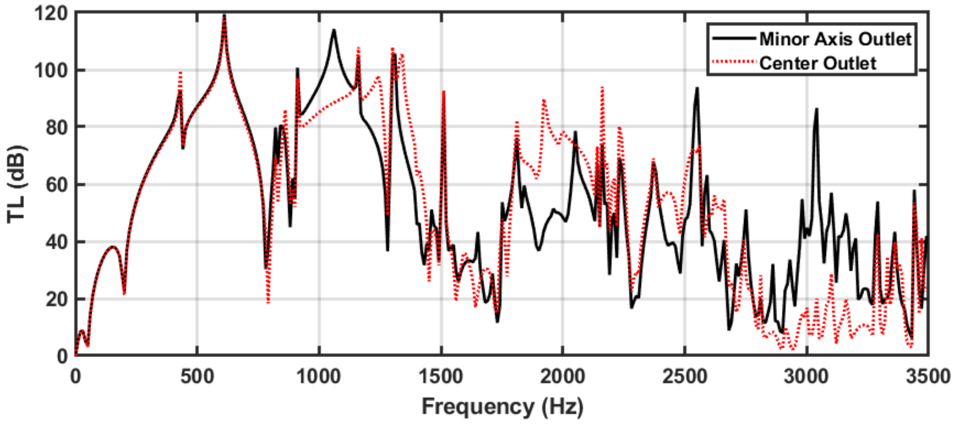

Figure 4.18: Comparison of TL between the configuration 1(a) and configuration 1(b).

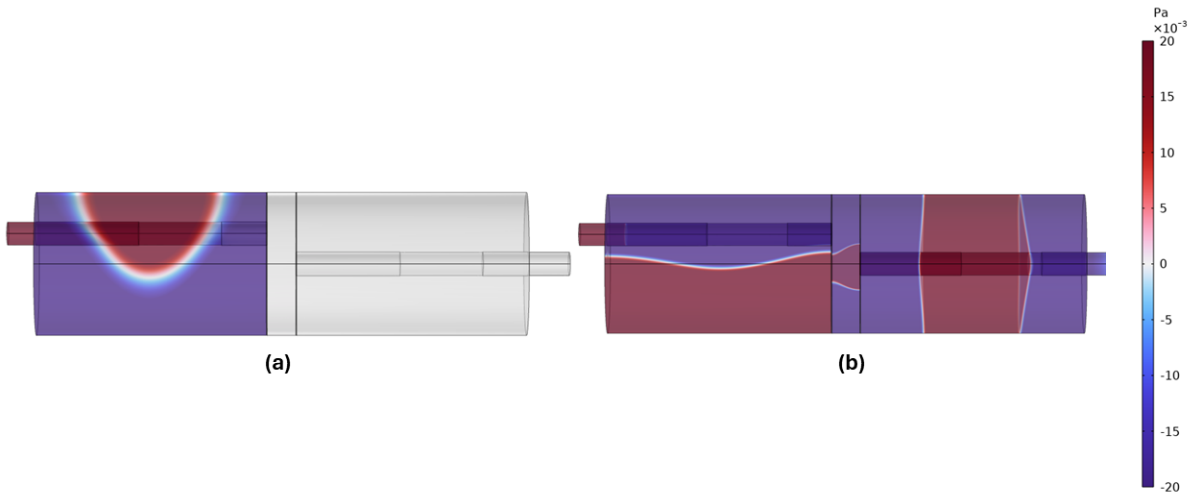

Figure 4.19: Total acoustic pressure variation for configuration 1 (a) and 1 (b) at two different frequencies.(a) 611 (Hz) and (b) 781 (Hz).

Figure 4.20 shows the comparison of transmission loss spectra from the numerical analysis for configuration 2 (a) and configuration 2 (b). Both configurations give the same transmission loss up to 1000 Hz, after that, both are very close to each other and follow the same trend but between 1600-1900 Hz, small variations are there but after 1900 Hz both the TL spectra follow the same variation.

From Fig. 4.20 the highest TL value for configuration 2 (a) and configuration 2 (b) is 110 dB at 611 Hz and subsequently the trough is coming up to 40 dB at the 781 Hz. The reason for the highest TL value can be seen in Fig. 4.21(a) that, the impedance for the frequency 611 Hz is very small and the total acoustic pressure at the outlet of the muffler configuration is zero. The reason for the trough in the TL at 791 Hz can be seen in Fig. 4.21(a) that, the impedance for the frequency 791 Hz are high and the total acoustic pressure at the outlet of the muffler configuration is high.

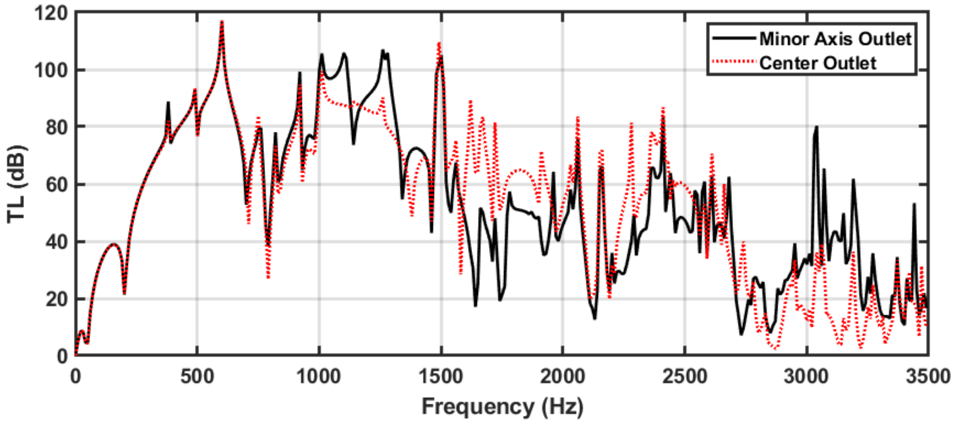

Figure 4.20: Comparison of TL between the configuration 2(a) and configuration 2(b).

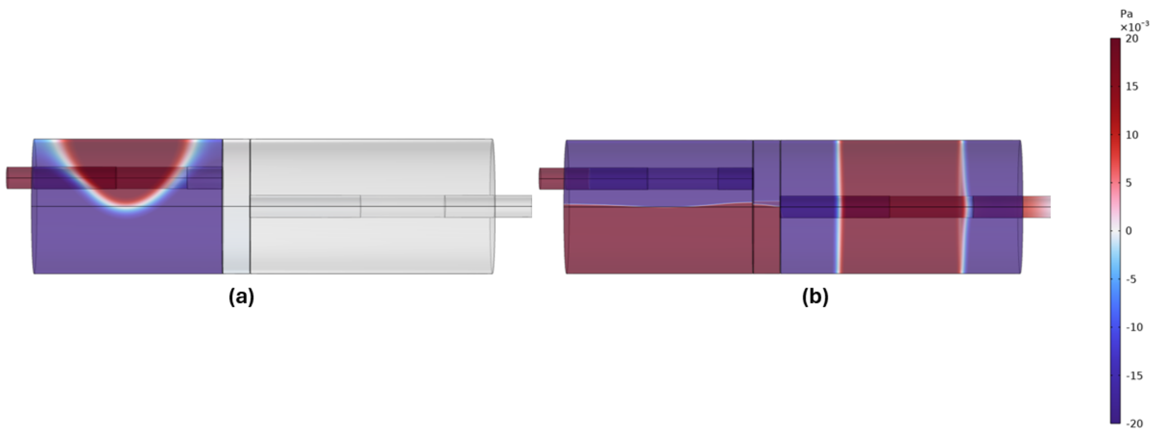

Figure 4.21: Total acoustic pressure variation for configuration 2 (a) and 2 (b) at two different frequencies.(a) 611 (Hz) and (b) 791 (Hz).

Figure 4.22 shows the comparison of TL spectra from the numerical analysis for Configuration 1(a) and Configuration 2(a) both have major axis inlet and center outlet, but the dimensions are different. Configuration 1(a) have two same length of eccentric extended perforated tube muffler with the short chamber muffler, while The configuration 2 (a) have two different length of eccentric extended perforated tube muffler with the short chamber muffler. The first peak are coming in configuration 1 (a) at 428 Hz because of the L_{a1} resonator. but in Configuration 2(a) eccentric extended perforated tube mufflers have different lengths, because of that two different lengths of quarter-wave resonators are there, that is why two peaks occurred, the first peak is coming because of the resonator L_{c1} at 381 Hz and the second peak are coming because of the resonator L_{a1} at 490 Hz. Configuration 1 (a) and configuration 2 (a) have the same TL spectra up to the frequency 381 Hz after that there was a little variation of the peak, and further both the muffler's TL spectra are very close to each other.

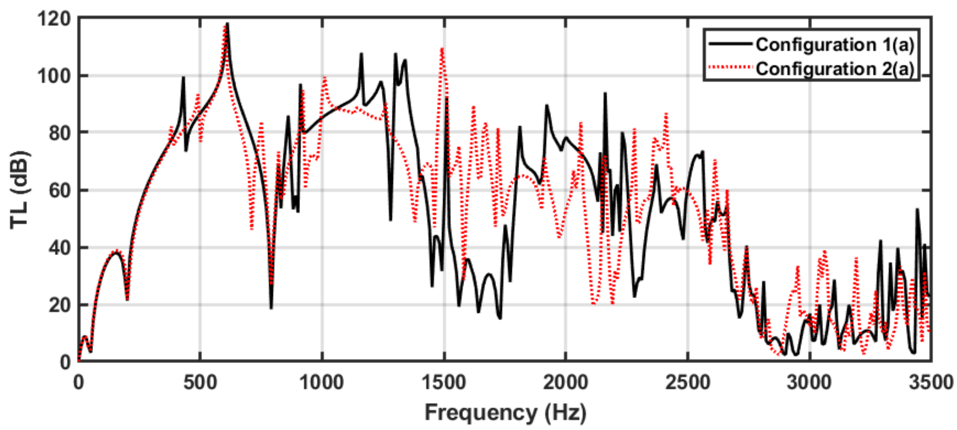

Figure 4.22: Comparison of TL between the configuration 1(a) and configuration 2(a).

Figure 4.23 shows the comparison of transmission loss spectra from the numerical analysis for Configuration 1 (b) and Configuration 2 (b) both have major axis inlet and minor outlet, but the dimensions are different. Configuration 1 (b) has two same lengths of eccentric extended perforated tube muffler with the short chamber muffler, while configuration 2 (b) has two different lengths of eccentric extended perforated tube muffler with the short chamber muffler. The first peak is coming in Configuration 1 (b) at 428 Hz because of the L_{a1} resonator, but in Configuration 2(b) eccentric extended perforated tube mufflers have different lengths, because of the two different lengths of quarter wave resonator are there, that is why two peaks occurred, the first peak is coming because of the resonator L_{c1} at 381 Hz and the second peak are coming because of the resonator L_{a1} at 490 Hz. Configuration 1 (b) and configuration 2 (b) have the same TL spectra up to the frequency 381 Hz after that there was a little variation of the peak are there, and further both the muffler's TL spectra are very close to each other.

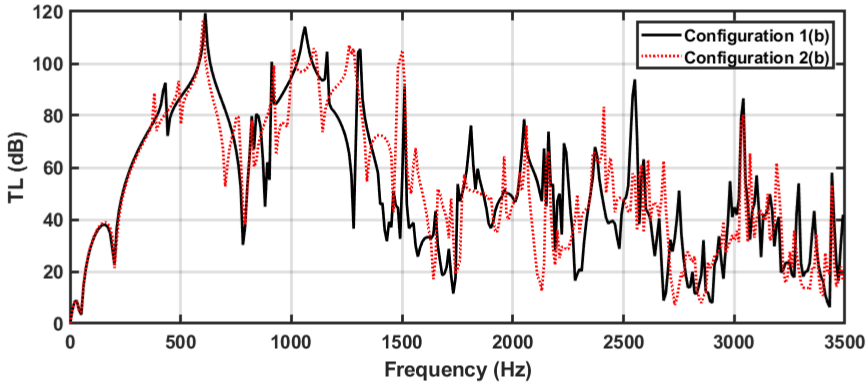

Figure 4.23: Comparison of TL between the configuration 1(b) and configuration 2(b)

The comparison of the TL spectra with the same length for the simple expansion chamber muffler, double-tuned extended inlet outlet muffler and double-tuned extended concentric tube resonator muffler are shown in figs. 4.24 to 4.27. The value of the transmission loss is very high for the designed configurations and have a wide-band working range.

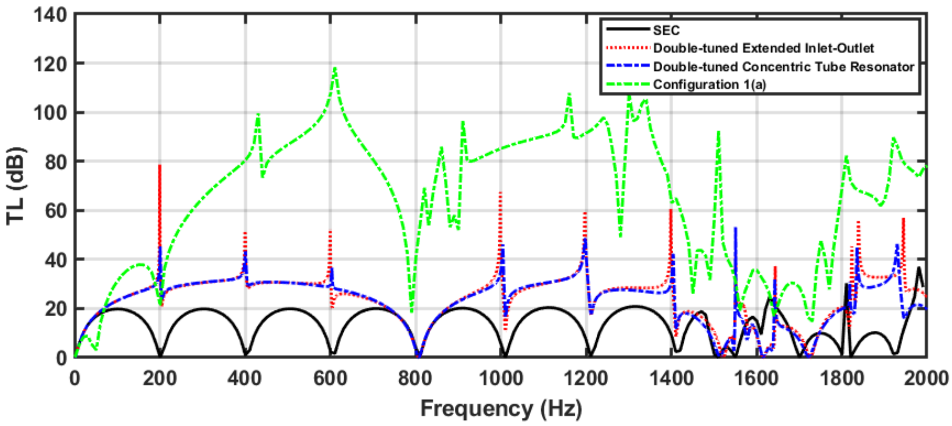

Figure 4.24: Comparison of TL for configuration 1(a) between SECM, double tuned extended inlet outlet muffler and double tuned concentric tube resonator muffler.

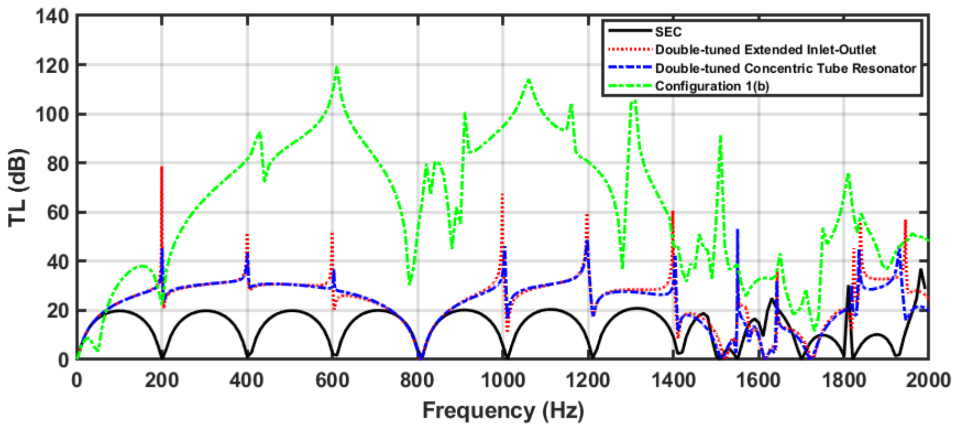

Figure 4.25: Comparison of TL for configuration 1(b) between SECM, double tuned extended inlet outlet muffler and double tuned concentric tube resonator muffler.

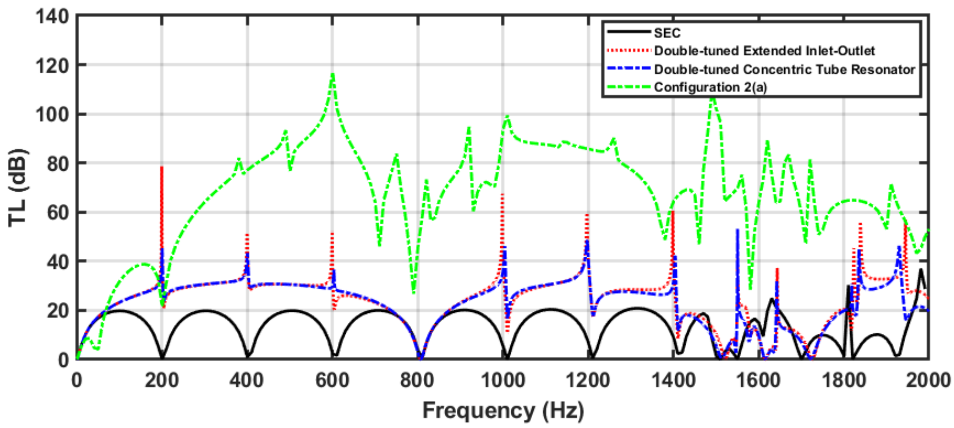

Figure 4.26: Comparison of TL for configuration 2(a) between SECM, double tuned extended inlet outlet muffler and double tuned concentric tube resonator muffler.

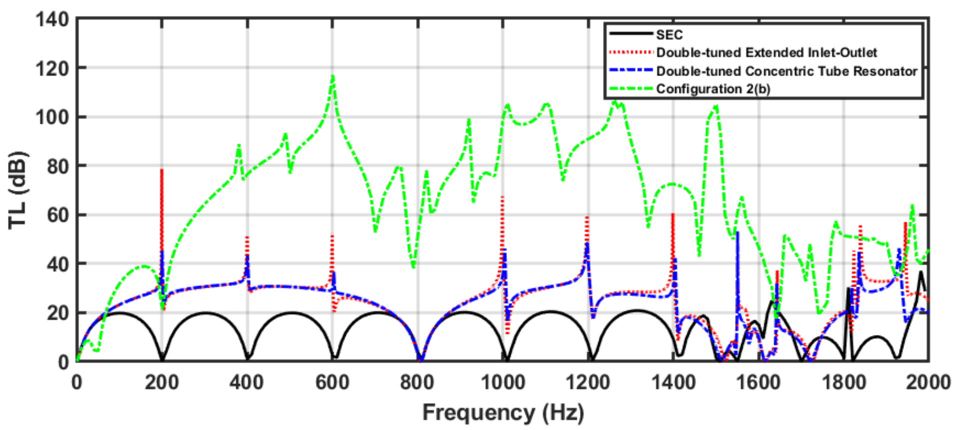

Figure 4.27: Comparison of TL for configuration 2(b) between SECM, double tuned extended inlet outlet muffler and double tuned concentric tube resonator muffler.

Chapter 5

Conclusions and Scope of Future work

This chapter summarizes the present work study, the effectiveness of all the designed muffler configurations, and the range of working and also recommend for future work that can be done to improve the performance of the mufflers.

5.1 Conclusions

- The goal of the proposed study was to build a muffler with high transmission loss in the low frequency, a wide band working range, and less back pressure.

- The study was initially focused on the variation in TL spectra for extended concentric tube resonator mufflers, variation of the port location in eccentric extended perforated tube resonator mufflers, and short chamber mufflers with different port locations. The transmission loss spectra for each muffler were observed closely. Further, the muffler was studied in detail and the model was prepared by a combination of the two eccentric extended perforated tube resonator mufflers with the short chamber muffler.

- Four different types of muffler configurations are design by combining eccentric extended perforated tube resonator muffler with short chamber muffler.

- The reason of the poor performance in the designed muffler configurations, when the outlet port are placed at the major axis is because of the $(1, 1)_{even}$ mode are getting excited into the short chamber muffler.

- From Fig. 4.18, the maximum transmission loss for the Configuration 1 (a) and configuration 1 (b) are found to be 70 dB in between the frequency range 250 Hz - 700 Hz, 40 dB in between the frequency range 250 Hz - 1400 Hz, 20 dB in between the frequency range 90 Hz - 1700 Hz.

- From the Fig. 4.20 the maximum transmission loss for the Configuration 2 (a) and configuration 2 (b) are found to be 70 dB in between the frequency range 300 Hz - 600 Hz, 40 dB in between the frequency range 190 Hz - 1600 Hz, 20 dB in between the frequency range 90 Hz - 2100 Hz.

- As per the lumped flow resistance network theory the head loss in the simple expansion chamber muffler, the double-tuned extended inlet and outlet muffler, and all the designed muffler configurations are the same (1.5 m) because of sudden expansion and contraction, but the transmission loss spectra for all the designed configurations are very high as well as wideband as compare to the simple expansion chamber muffler and the double tuned extended inlet and outlet muffler with the same chamber length which are shown in Fig 4.10 to 4.13.

5.2 Recommendations for future work

All the designed muffler configurations are effective but not that much significant in the high-frequency region and also sudden troughs are coming in some frequency range, so, future efforts might be focused on the following areas:

- Huang et al.[22] have done the analysis on the three pass perforated tube duct muffler which are shown in Fig. 5.1 with and without the use of the sound absorbing material and evaluate the changes in the TL spectra.

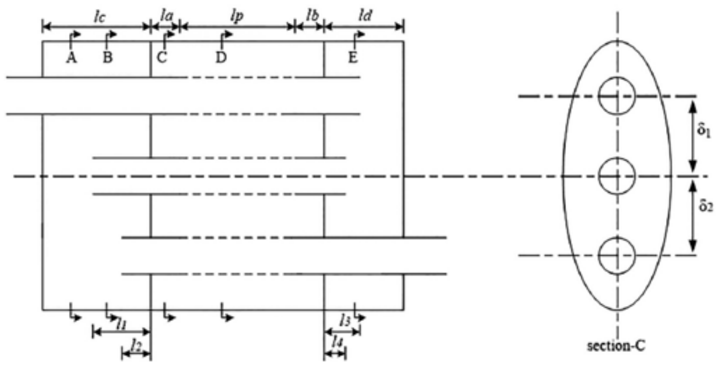

Figure 5.1: Three-pass perforated tube muffler (baseline configuration)

- Thus, the impact of sound-absorbing material on the TL spectra can be seen in Fig. 5.2, where an increase in the material results in an increase in the TL spectrum, and also there is no compromise in the low-frequency range. Thus the Sound-absorbing material can be added to the proposed muffler designs and observe to the change in TL spectra.

- To evaluate the TL spectra and IL spectra at different mean flow value for all the designed configurations.

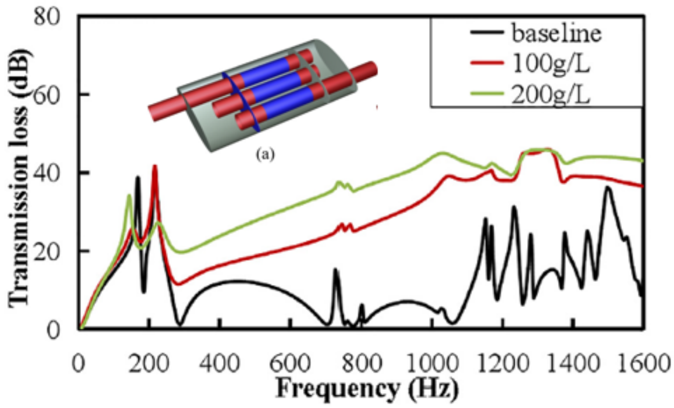

Figure 5.2: Effect on transmission loss by adding sound-absorbing material in three-pass perforated tube muffler

References

[1] https://www.alamy.com/stock-photo-diagram-illustrating-noise-flow-through-a-typical -muffler-24898293.html.

[2] E. Dokumacı. *Duct acoustics: fundamentals and applications to mufflers and silencers.* Cambridge University Press., (2021).

[3] M. L. Munjal. *Noise and vibration control. (Vol. 3)*. World Scientific, (2013).

[4] M. L. Munjal. *Acoustics of ducts and mufflers*. John Wiley & Sons, (2013).

[5] A. Selamet and Z.L. Ji. "Acoustic attenuation performance of circular expansion chambers with extended inlet/outlet". In: *Journal of Sound and Vibration* 223.2 ((1999)), pp. 197–212.

[6] F. C. Karal. "The analogous acoustical impedance for discontinuities and constrictions of circular cross section". In: *The Journal of the Acoustical Society of America* 25.2 (1953), pp. 327–334.

[7] A.D. Sahasrabudhe, M.L. Munjal, and S. Anantha Ramu. "Analysis of inertance due to the higher order mode effects in a sudden area discontinuity". In: *Journal of Sound and Vibration* 185.3 (1995), pp. 515–529.

[8] A.J. Torregrosa, R. Broatch, and Gonza lez. "Numerical estimation of end corrections in extended-duct and perforated-duct mufflers". In: ((1999)).

[9] M.L. Munjal and S. Gowri. "Theory and design of tuned extended-tube chambers and concentric tube resonators". In: *Journal of Acoustic Society of India* (2009), pp. 53–71.

[10] P. Chaitanya and M.L. Munjal. "Effect of wall thickness on the end corrections of the extended inlet and outlet of a double-tuned expansion chamber". In: *Applied Acoustics* 72.1 (2011), pp. 65–70.

[11] P. Chaitanya and M.L. Munjal. *Tuning of the extended concentric tube resonators*. Tech. rep. SAE Technical Paper, (2011).

[12] E. Ramya and M.L. Munjal. “Improved tuning of the extended concentric tube resonator for wide-band transmission loss”. In: *Noise Control Engineering Journal* 62.4 (2014), pp. 252–263.

[13] K. M. Kumar. “On the crucial role of higher order evanescent modes for double-tuning ofsame-end inlet-outlet and opposite-ends inlet-outletelliptical chamber mufflers”. In: *Applied Innovative Research,* 4 (2023), pp. 252–263.

[14] F.D. Denia, J. Albelda, and Fuenmayor. “Acoustic behaviour of elliptical chamber mufflers”. In: *Journal of Sound and Vibration* 241.3 (2001), pp. 401–421.

[15] A. Selamet and F.D. Denia. “Acoustic behavior of short elliptical chambers with end central inlet and end offset or side outlet”. In: *Journal of sound and vibration* 245.5 (2001), pp. 953–959.

[16] A. Mimani and M.L. Munjal. “Transverse plane wave analysis of short elliptical end-chamber and expansion-chamber mufflers”. In: *International Journal of Acoustics and Vibration* 15.1 (2010), p. 24.

[17] A. Mimani and M.L. Munjal. “Transverse plane wave analysis of short elliptical chamber mufflers: An analytical approach”. In: *Journal of sound and vibration* 330.7 (2011), pp. 1472–1489.

[18] https://group.met.com/en/mind-the-fyouture/mindthefyouture/when-will-fossil-fuels-run-out. *WHEN WILL FOSSIL FUELS RUN OUT?* METGroup Countries, 2015.

[19] https://www.ncbi.nlm.nih.gov/pmc/articles/PMC10357457/. *The Actual Toxicity of Engine Exhaust Gases Emitted from Vehicles*. 2023.

[20] A. Mimani. *Acoustic analysis and design of short elliptical end-chamber mufflers*. Springer, 2021.

[21] N.K. Vijayasree and M.L. Munjal. “On an Integrated Transfer Matrix method for multiply connected mufflers”. In: *Journal of sound and Vibration* 331.8 (2012), pp. 1926–1938.

[22] H. Huang, Z. Ji, and Z. Li. “Influence of perforation and sound-absorbing material filling on acoustic attenuation performance of three-pass perforated mufflers”. In: *Advances in Mechanical Engineering* 10.1 (2018), p. 1687814017748012.